LHC Project Note 10

1995-10-11

(PERINID @ CERNVM.CERN.CH)

Finite Element Structural Analysis of LHC Bending Magnet (version with 180 mm beam spacing)

A. Maffezzoli, D. Perini, J. Salminen and J. Soini

Keywords: DIPOLE, DISPLACEMENT, STRESS, TOLERANCES

1. INTRODUCTION

Finite element calculations have been carried out for the 56mm bore twin aperture superconducting LHC dipole prototypes with an aluminum common collar, and a vertically split yoke. The structure has been studied during the assembly at room temperature, at 1.8K non-energized, and energized. The ANSYS finite element package was used to compute the electro-magnetic (e. m.) forces at 9.7T. From this the same finite element package calculated the stress and strains present in the structure. Only the structural model is considered in this presentation. The aim of the optimization was to define the nominal dimensions so that favorable stresses can be obtained under all load cases. The vertical gap between yoke halves must be closed before and after the magnet is energized, and a good contact is needed between collars and yoke to ensure as rigid a structure as possible.

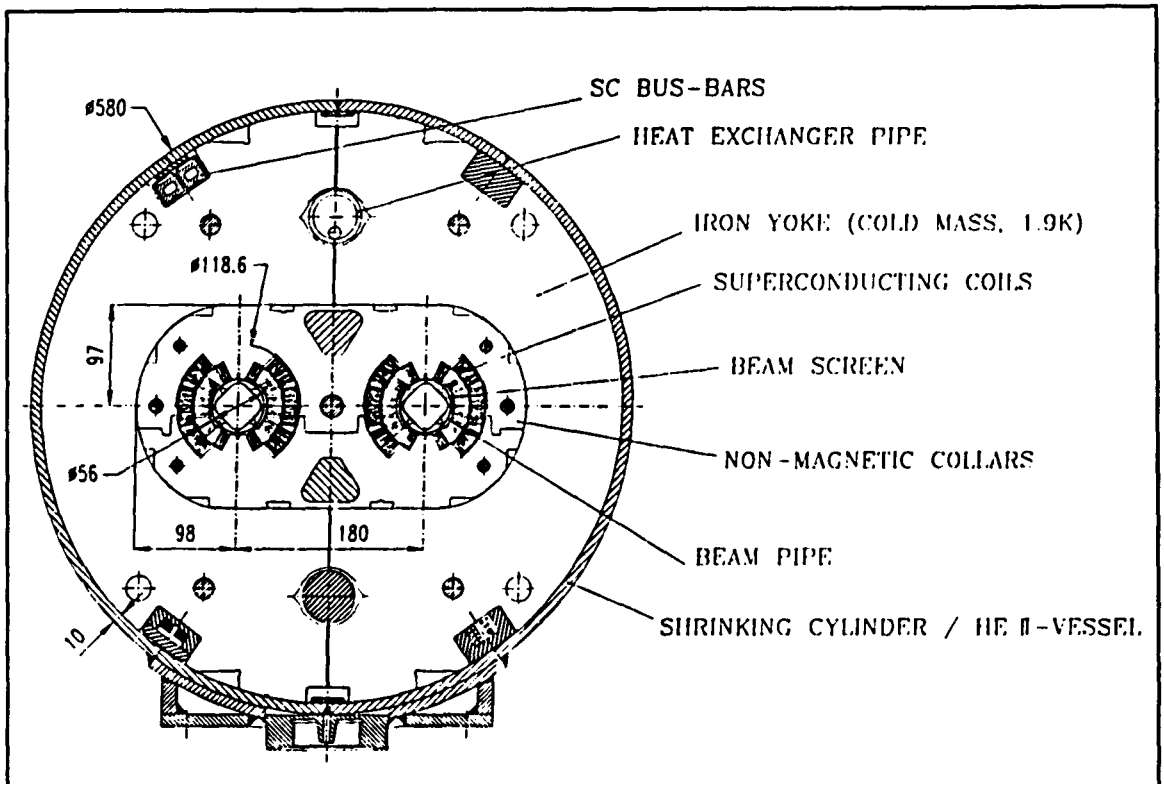

Figure 1. Cross-section of LHC-superconducting dipole magnet

2. FINITE ELEMENT-MODEL

A two dimensional model has been meshed and the plane stress option has been used in elements. Through the magnet's longitudinal section, every second collar is keeping the forces that are exerted by the coils. It is possible to simulate such a structure by creating two layers of 0.5mrn thick mesh for the collars. For the coils, iron yoke, cylinder and pins a 1 mm thick layer is meshed. The stiffness seen by a point-A (fig. 2) in positive y-direction is the same as seen by point-B in negative y-direction because of the symmetry of the structure. Using constrain equations ($\Delta yA=-\Delta yB$ and $\Delta xA=\Delta xB$) for the nodes laying on the horizontal axis, it is possible to imitate the behavior of the collars by modeling a quarter of the magnet cross-section.

The prestress of the coils is imposed by giving an interference at the interfaces between the collars and the coil heads.

The external cylinder prestress is also simulated by giving an interference between the iron yoke and cylinder interface.

The geometry is modeled at room temperature and in non-deformed conditions. That is to say the dimensions used in the model are for parts in their nominal size.

The areas have been meshed using two dimensional linear 42-elernents and contact surfaces with three dimensional 52-contac elements. Further information concerning these elements are available from the ANSYS-manuals.

Energization of the magnet is simulated by loading the coils with the electro-magnetic (e. m.) forces computed with the same code. Iron saturation has been taken into account.

No friction at all has been considered.

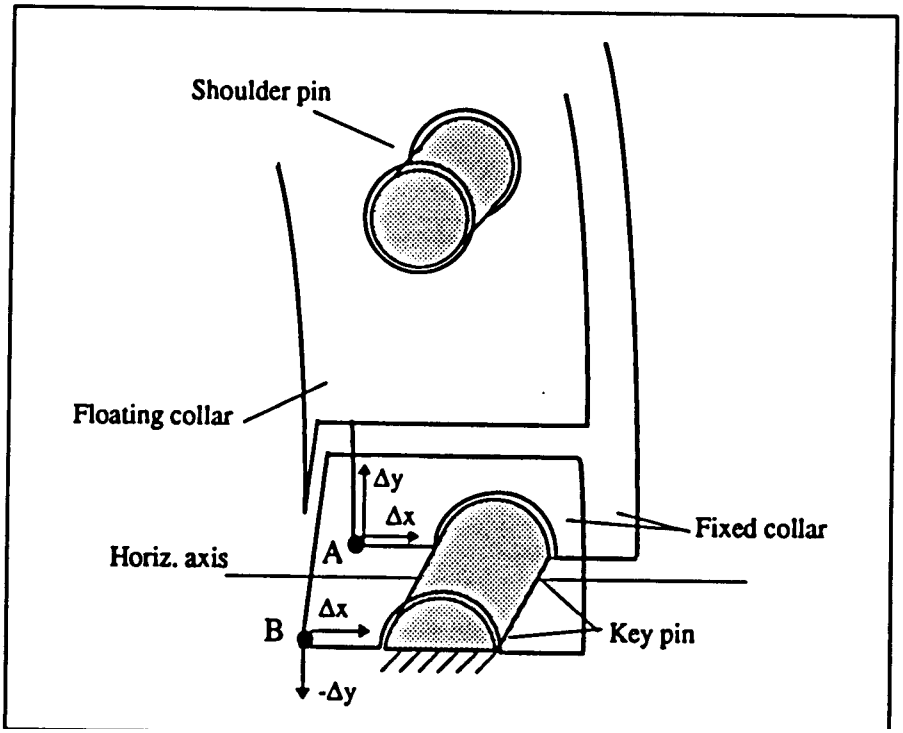

Figure 2. Constrain equations to simulate two collar layers

3. MATERIAL PROPERTIES

The material properties are listed in table 1. For the coil which compounds, cable and insulation, we used an equivalent Young's modulus.

	Thermal contraction [K^{-1}]	Young's modulus [MPa]		Allowable stress [MPa]	
Material	α 293-4.2K	293K	1.8K	293K	1.8K
Aluminium	$4.2x10^{-3}$	70000	81000	100	150
Iron yoke	$1.98x10^{-3}$	210000	225000	70	150
St steel	$2.95x10^{-3}$	180000	210000	200	400
Coils rad	$4.16x10^{-3}$	50000	50000	-120	-150
Coils azim	$4.16x10^{-3}$	15000	18000	-120	-150
Copper	3.26x10-	120000	150000	150	150

Table 1. Material properties

4. COLLARING

4.1 GENERAL

During the collaring, the collars are assembled with a given interference around the coils. The compression of the coils reaches the maximum value under the press just before the insertion of the pins. Once the pins are in, and the pressure is released, part of the compression is lost, because of the deformation of the collars.

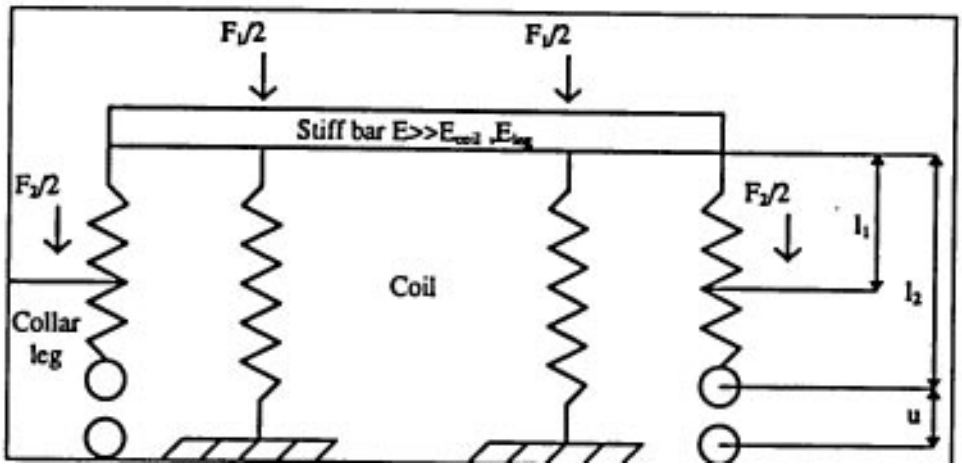

Figure 3. Coils and collar presented as springs.

In order to limit the stresses in the coils under the press, it is necessary to elongate the collar legs during the collaring process. This is obtained by pushing on the slots in the collars. If for sake of simplicity all non-linear phenomena are ignored the coil-collar structure of one aperture can be simulated using springs.

If the collaring force is applied at the top of the collars, the coils have to deform by length u, to allow us to insert the locking rods. If we mark the spring constant of the coil with k_{coil}, the force needed to insert the rods is therefore:

$$F1 = 2 \cdot u \cdot kcoil$$

If the collaring force is applied only on the side of the collars the force that is needed will be:

$$F2 = \frac{2 \cdot u \cdot kcoil}{1 + \frac{kcoil}{kcollar}}$$

Where k_{collar} is the spring coefficient of the collar legs. Since the central post of the collar is much stiffer than the legs, most of the spring back effect is the result of the legs elasticly deforming and the local deformation around the pins. When the press is released and the locking pins are placed, the compression force in the coil is taken by the length 'l_2'. Therefore relaxation of the stress in the coil is smaller if we press close to the horizontal axis. However, it is not possible to push only at the extreme edges of the collars, since stresses might become excessive due to the fact that we have not enough surface area to apply the forces to. Therefore it is necessary to apply an additional collaring force at the top of the collars.

The collaring process has been simulated for two cases: with the press applying load to the collars, this permits the key pins to be inserted and, after the pins have been inserted and the press released.

In the first load step the required collaring pressure to superimpose the keypin holes is defined. This is done by fixing the upper edge of the tool in the vertical direction (fig. 4) and placing shims (interference) between tool and collars, so that the keypin holes overlap. The vertical reaction force corresponds to the required collaring force. In the second load step the validity of the previous model has been shown by releasing the upper edge of the tool, applying the collaring force and converting the interference to an equivalent gaps (rig. 5 and table 2). The third model represents collared coil after the pins have been introduced and the press released. To eliminate the different displacements in the key pin holes, after the first load step (table 2) the collars are locked in this position.

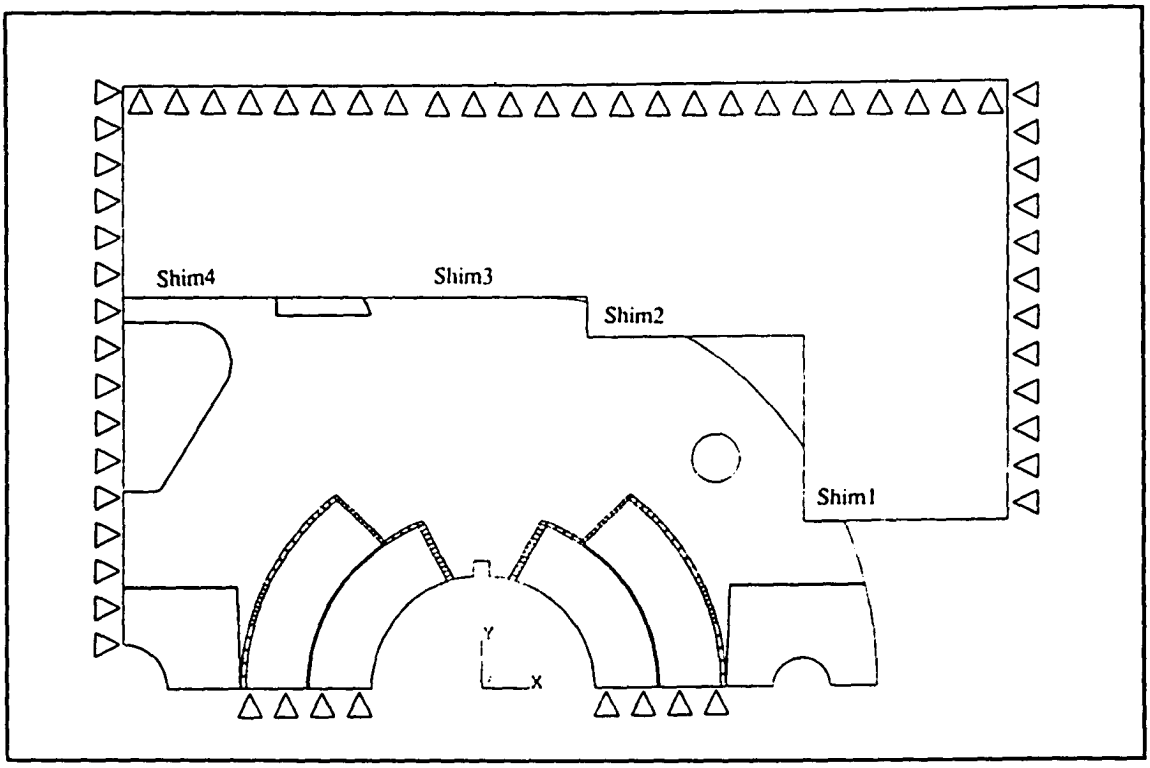

Figure 4. The collaring model. In the first load step, the top of the tool has been fixed to define the required collaring force.

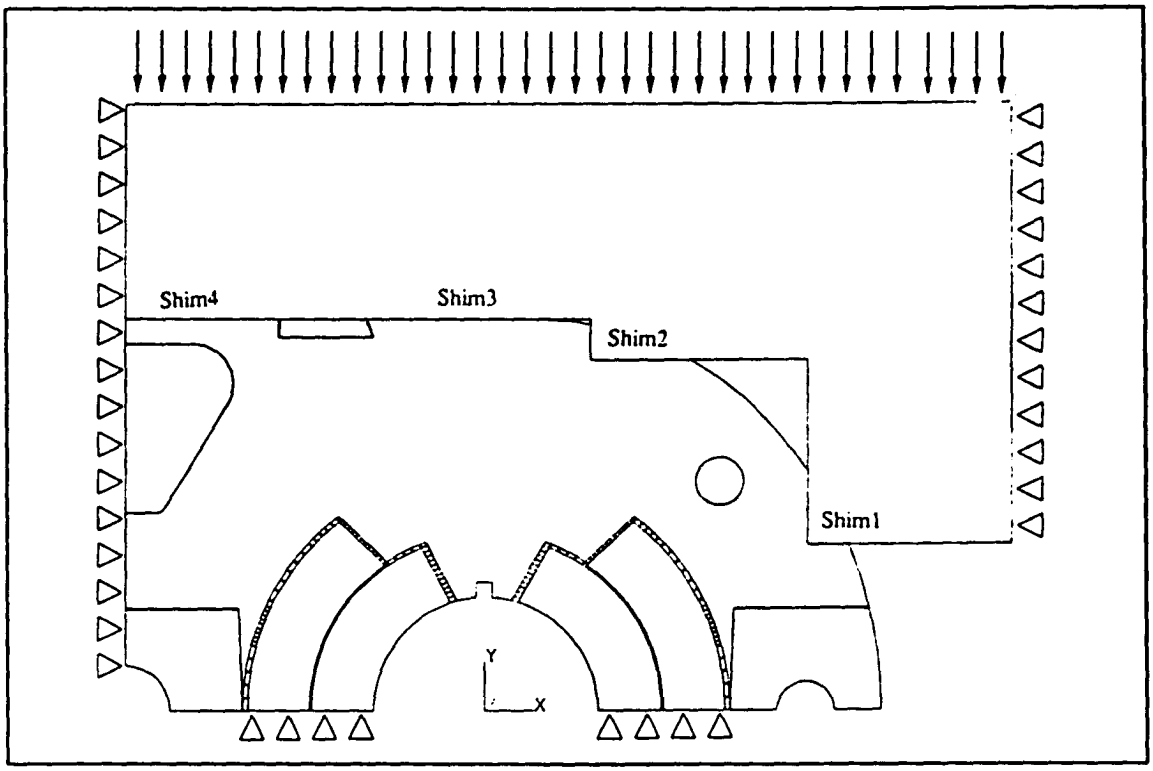

Figure 5. The collaring model. In the second load step the previously obtained collaring force is applied at the top of the tool. In the third load step (not shown). the pins are inserted and press released.

	1st load step Fixed tool edge	2nd load step (check)	3rd load step Press released	Reference case 1st load step	Reference case 3rd load step
Shims [mm]					
Shim1	-0.06	0	--	0	--
Shim2	0	0.06	--	-0.1	--
Shim3	1	1	--	1	--
Shim4	-0.02	0.04	--	-0.02	--
Forces [N/mm/½ collar]					
At top of the tool	-5199.8 (constrain)	-5199.8	--	-5627.8 (constrain)	--
Coil right (hor plane)	2541.5	2545.3	1313.6	2626.7	1271.8
Coil left (hor plane)	2658.3	2654.5	1139.3	3001.1	1145.3
Total Fy	5199.8	5199.8	2452.9	5627.8	2417.1
Coil stresses along the coil mid plane [MPa]					
$\sigma_{average}$	84.4	84.4	39.8	91.4	39.2
σ inner coil right	85.8	85.9	41.6	86.8	40.3
σ inner coil left	90.5	90.4	37.4	104.5	37.3
σ outer coil right	79.2	79.3	43.7	83.8	42.3
σ outer coil left	82.1	82.0	36.6	90.4	37.1
Vert. offset of locking rod center from hor. axis [mm]					
Right	-1.1×10^{-3}	-1.4×10^{-3}	--	-0.0125	--
Left	-7.3×10^{-3}	-7.2×10^{-3}	--	-3.8×10^{-3}	--

Table 2. Study of the collaring process. Negative values mean interference. All forces are for one coil (a half collar) per mm.

The coils prestress reported in table 2 is the minimum value imposed after collaring in order to avoid tensile stress in the coils during energization. A margin is given by the fact that the considered field for the computations is 9.7T; a further margin can be given increasing the prestress after collaring. It is in any case important to stay below the limit of 120MPa under the

We can define a relaxation ratio as a ratio between the vertical constrain forces in the coils, on horizontal axis after (Fyls3) and before (Fyls1) the press is released.

press.

$$\frac{F_{yls3}}{F_{yls1}} = \frac{1313.6 + 1139.3}{2541.5 + 2658.3} \approx 47.2\%$$

From table 2 it can be seen that the relaxation ratio of the left coil is lower than that for the right coil. This is due to the fact that there is higher stress concentration near the left key pin and consequently higher deformation at this point.

To show the advantage of preloading the collar legs, we have calculated a reference case where only the top of the collar has been pressed this is shown in the table 2.

The relaxation is:

$$\frac{r_{yls3}}{F_{yls1}} = \frac{1271.8 + 1145.3}{2626.7 + 3001.1} = 42.9\%$$

This means that the relaxation can be reduced by 4.3% by elongating the collar legs during the collaring process.

5. ASSEMBLY OF THE MAGNET

The maximum vertical displacement (0.268mm) in the collared coil pack occurs at the vertical symmetry plane above the iron insert (fig. 7 in appendix). Elsewhere the displacements at the top of the fixed collars are 0.14-0.18mm. To avoid the need for special tooling the shape of the iron yoke must take into account the deformed shape of the collars after the collaring.

It is possible to deform the 'C' shaped yoke by a maximum of 0.23mm in each half before the azimuthal tensile stresses near the horizontal plane become excessive (i.e. 0.23mm vertical displacement of the point x0 gives rise to 100MPa tensile stress at the point E (fig. 6)). The gap size between x0-x38 is 0.2mm (fig. 6). In this way the collar assembly can be placed into the yoke, only in the final stages of the assembly a small interference of 0.07mm between yoke and the collar appears.

6. THE COMPLETE MAGNET

6 1 GENERAL

To avoid any conductor movement under the influence of the electro-magnetic (e. m.) forces, the conductors must be well supported when the magnet is energized. During Energization the e. m. forces will unload the pressure between the center post and the first turn of the coil. When the magnet is energized some azimuthal compression is needed to ensure that no cracks or sudden displacements occur in the coils. On the other hand to avoid the deterioration of the coil through creep the room temperature prestress should not be too high [4].

During cool down from room temperature to 1.9K the iron contracts much less than the collars. To compensate for the different contractions, there is a vertical gap in the iron. This gap permits the iron to follow the collars contraction and so maintain a good contact

6.2 DISCUSSION OF THE RESULTS

The assembled magnet has been analyzed at room temperature, at 1.9 K, B0 = 0 T and at 1.8 K, B0 = 9.7 T.
The parameters, stresses and displacements of the structure in the considered different load steps are reported in the tables 3-6 and figure 6.

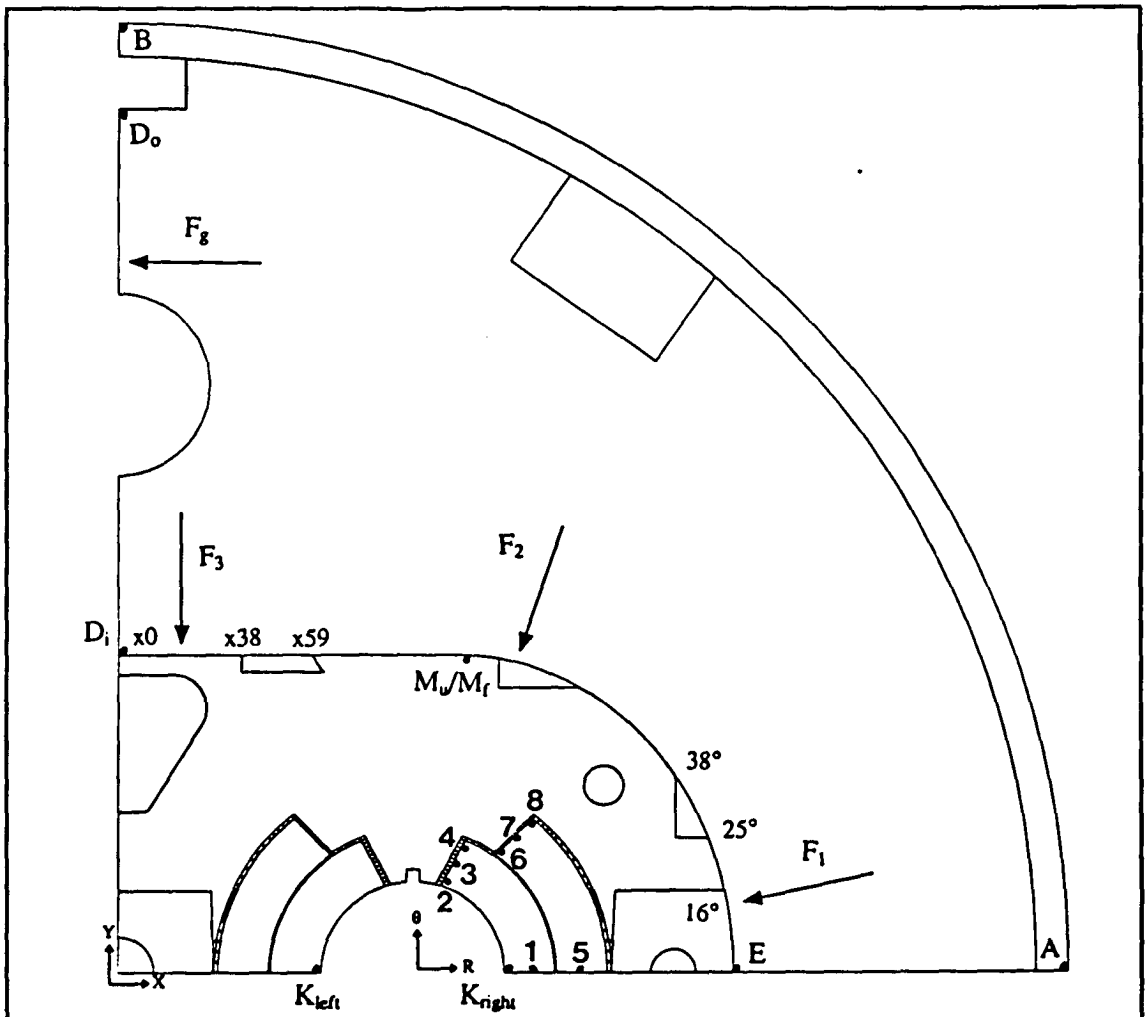

Figure 6. Parameters for the mechanical optimization and significant points.

Vertical gap size/half gap		
at the top (D_u)	0.62	mm
at the bottom (D_l)	0.47	mm
Collar-yoke gap size		
bottom at 0°	0	mm
at 25°	0.04	mm
at 38°	0.3	mm
x=59	0.3	mm
x=38	0.2	mm
x=0	0.2	mm
Shims		
inner coil r=28	0.28	mm
inner coil r=45.2	0.3	mm
outer coil r=45.7	0.3	mm
outer coil r=62.9	0.33	mm
Collar nose slot		
width/height	4x3.8	mm
Yoke-shrinking cylinder		
radius interference	-0.43	mm

***Table* 3.** Optimized parameters of the mechanical design.

Load Step	293K 0T		1.8K 0T		1.8K 9.7T	
Displacement (mm)	x	y	x	y	x	y
Points	U_x	U_y	U_x	U_y	U_x	U_y
A	-0.199	0	-1.04	0	-0.995	0
B	0	-0.079	0	-0.793	0	-0.823
D_o	-0.276	-0.073	-0.620	-0.725	-0.620	-0.756
D_i	-0.237	-0.052	-0.47	-0.380	-0.470	-0.404
E	-0.189	0	-0.819	0	-0.768	0
K_{right}	-0.190	0	-0.531	0	-0.444	0
K_{left}	0.002	0	-0.250	0	-0.282	0
M_u*	-0.037	0.236	-0.413	-0.201	-0.408	-0.252
M_f*	-0.035	0.227	-0.413	-0.212	-0.408	-0.262

* Collars are divided into two layers: fixed (Mu*) and floating (Mf*)

Table 4. Displacements in the some significant points.

Load step	293K 0T	1.8K 0T	1.8K 9.7T	
Vertical gap				
Fg	0	1738	713	N/mm
N/16 elements in contact	0	16	10	
Size at top	0.34	0	0	mm
Size at bottom	0.23	0	0	mm
Collar-yoke interface				
N/19 (0°-25°) elements in contact	15	6*	15	
*Max gap is 0.003mm				
F1(0°-25°)	1673	552	1626	N/mm
F2(38°≤x≤59)	0	0	0	N/mm
F3(0≤x≤38)	1044	513	658	N/mm
Max. shrinking cylinder stress on horiz plane	156	230	226	MPa
Lorentz force in right coil quadr. (9.7T)				
Fx	0	0	2248	N/mm
Fy(out. layer)	0	0	-194	N/mm
Fy(inn. layer)	0	0	-823	N/mm

Table 5. Characteristic data of the mechanical design.

Point	293K 0T	1.8K 0T	1.8K 9.7T	1.8K 8.4T	
1	-71	-70	-94	-88	MPa
2	-113	-97	-54	-65	MPa
3	-81	-77	-42	-51	MPa
4	-11	-32	-22	-24	MPa
5	-60	-61	-98	-89	MPa
6	-114	-92	-45	-57	MPa
7	-62	-58	-24	-32	MPa
8	-26	-49	-25	-31	MPa

Table 6. **Azimuthal stresses in some significant points in the coils**

The nominal gap between yoke and collars quadrand increases as a function of the angle . The gap is zero at the horizontal plane (0º) and increases linearly to a size of 0.04mm at 25º. A gap of 0.3mm has been left from the point x38 to the point x59 in order to avoid contact during the assembly (fig. 6).

The vertical gap is open at the room temperature and completely closed at 1.8K. When the magnet is energized the gap remains closed.

At room temperature a relatively strong contact exists between collars and yoke (table 5). At the 1.8K the normal resulting force decreases due to the fact that the aluminum collars shrink more than the surrounding yoke.

Figures 7 and 8 show normal forces between collars and yoke interface at low temperature both in the energized and not energized state. It can be seen that the loads are mainly concentrated near to the 25º angle and near the horizontal axis. Negative angles represent fixed collar leg, which starts below the horizontal axis (fig. 6). At 9.7T the collars have line to line fit from -5º to 25º.

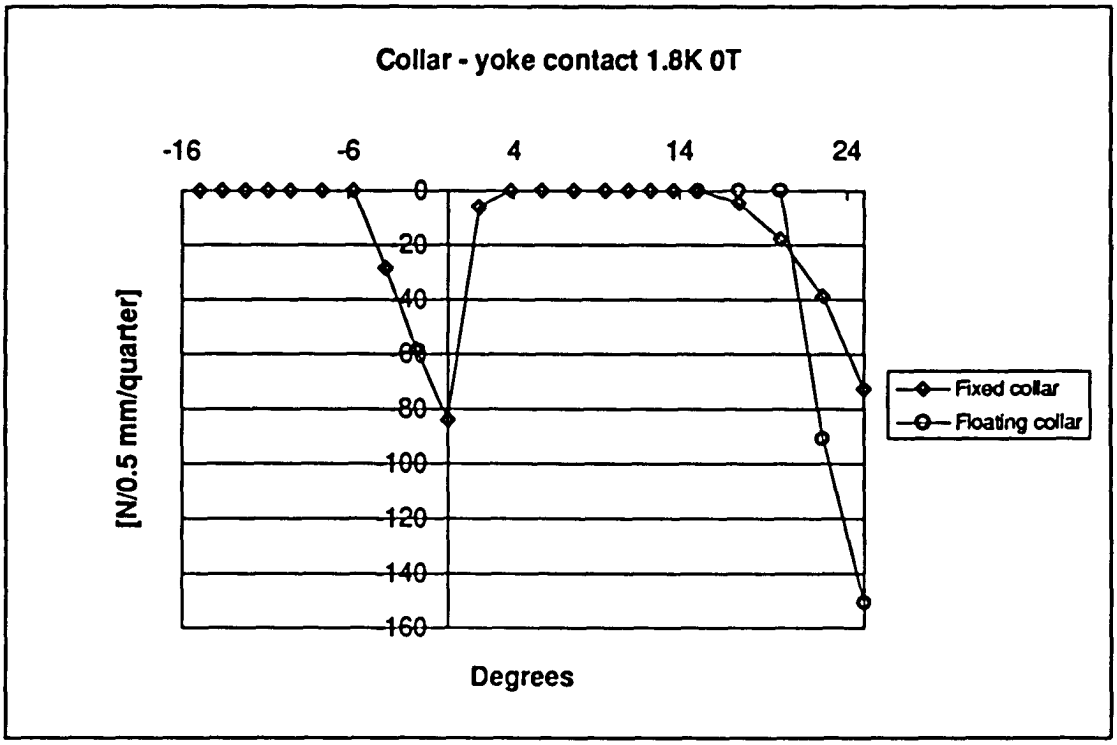

Figure 7. **Normal force between collar and yoke (-16° + 25°) at 1.8K and 0T in a quarter of the magnet.**

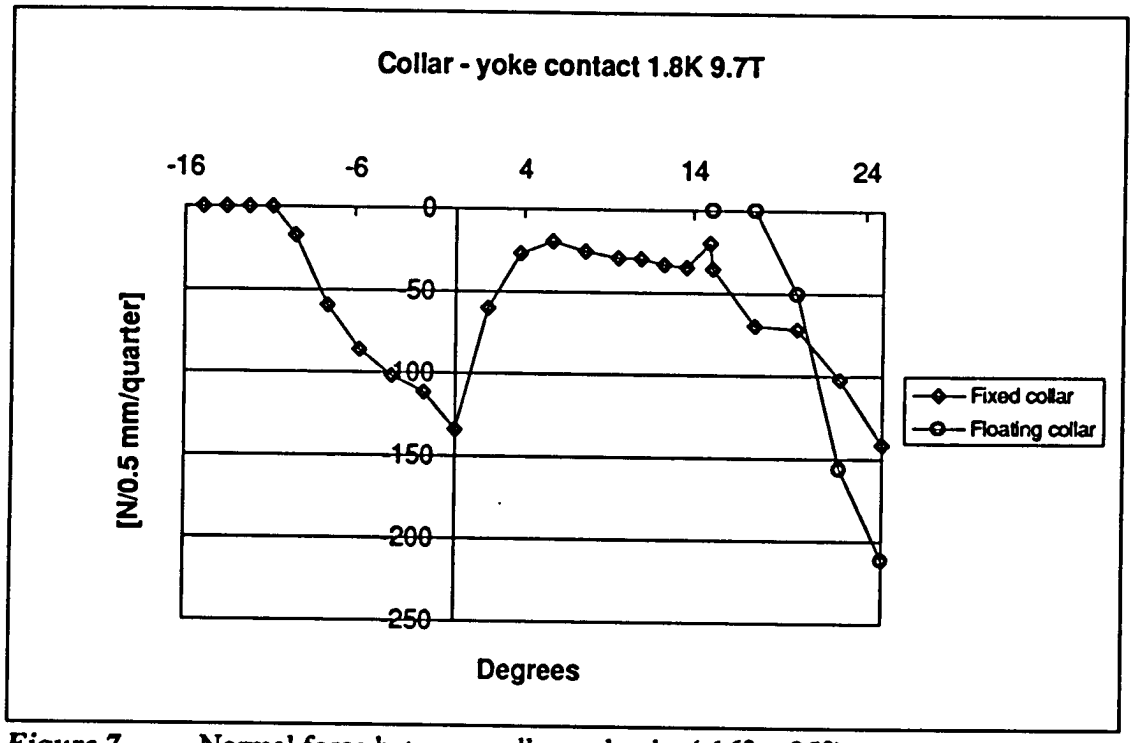

Figure 7. Normal force between collar and yoke (-16° + 25°) at 1.8K and 9.7T in a quarter of the magnet.

During the collaring the stress in the coils reaches its maximum value at room temperature. The compression is higher at the innermost corner of the top of the inner coil. Moreover the vertical gap is completely open at the room temperature, all the horizontal forces coming from the shrinking cylinder are taken by the collars. Part of this force is then transmitted to the coils. This increases the azimuthal stresses at the innermost corner of the top of the inner coils. In order to reduce these stresses a 3.8 deep and 4mm wide slot has been placed in the middle of the collar post (fig 9).

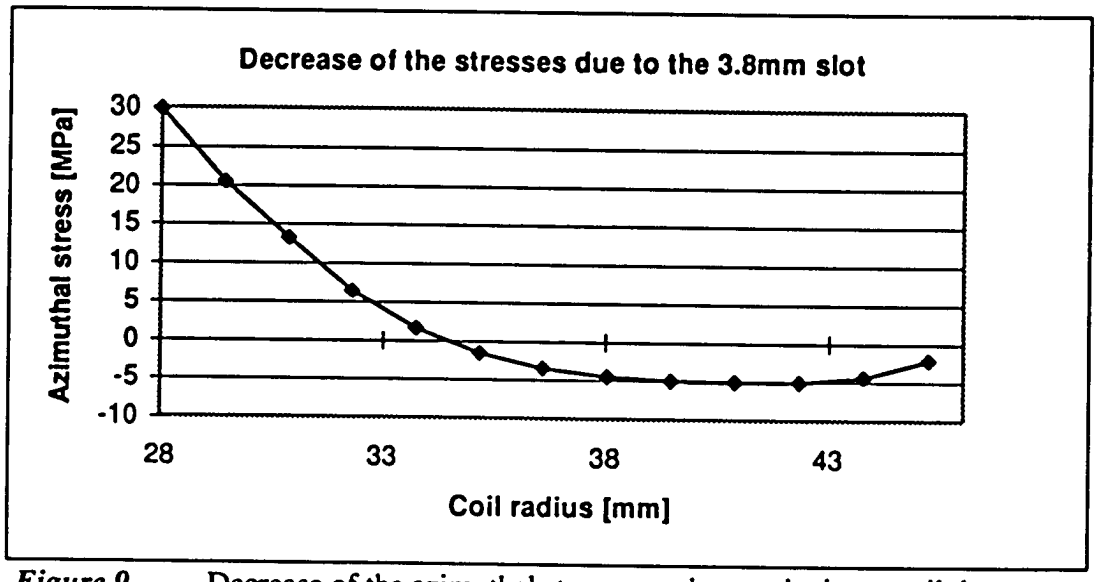

Figure 9. Decrease of the azimuthal stresses at the top the inner coil due to the 3.8mm slot.

7. TOLERANCES

Influences of the manufacturing tolerances on mechanical behavior of the magnet have been studied. To understand causalities and keep the number of the analysis reasonable only one parameter per time has been changed.

We changed following parameters see figure 5:

- Gap size between collar and yoke at 25º
- Gap size between collar and yoke from 0º to 25º
- Gap size between collar and yoke from x0 to x38
- Half vertical gap size between yokes from D_i to D_0.

Influence of the gap size at 25º on the normal forces is shown in the figure 10. The normal force F_1 between 0º-25º at 1.8K starts to show non-linear behavior when the gap size is bigger than 0.06min, due to lack of contact.

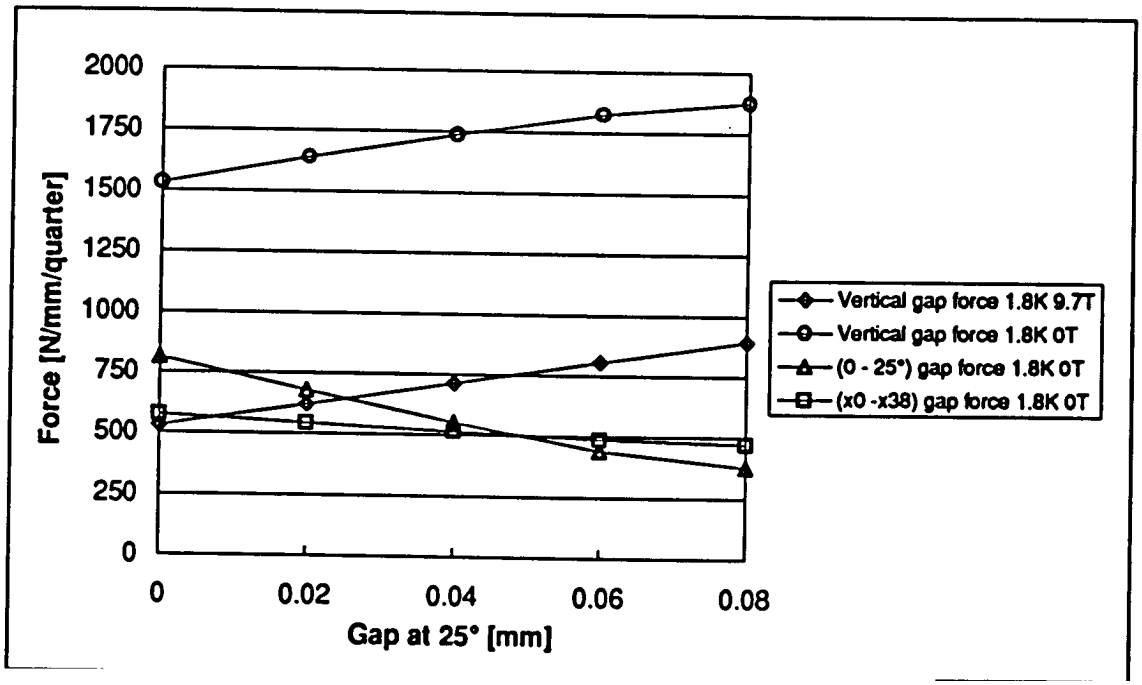

Figure 10. Normal contact forces between surfaces vs. gap size at 25º. Nominal gap size at 25º is 0.04mm.

Figure 11 presents the influence of the parallel shift of the gap between collar and yoke from 0º to 25º. One can see that the sum F_1+F_g. remains more almost constant at 1.8K within the tolerance area in question.

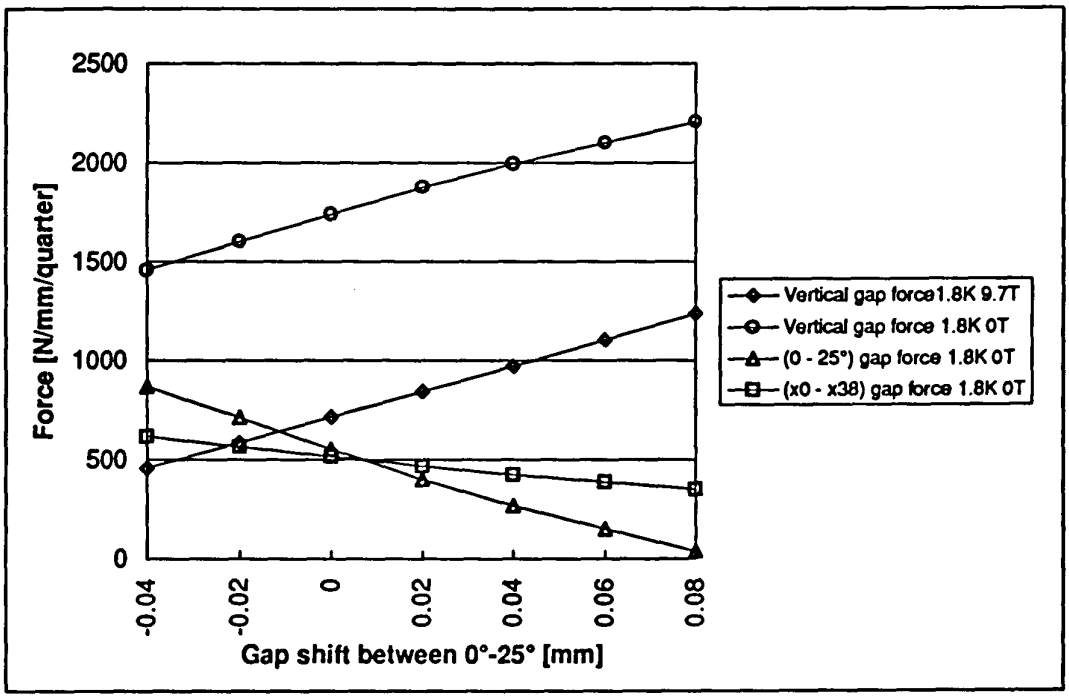

Figure 11. Normal contact forces between surfaces vs. parallel gap shift between 0^{o}-25^{o} Nominal gap size is 0mm at 0^{o} and 0.04mm at 25^{o}.

Vertical gap mating force F_g increases when the x0-x38 gap increases (fig. 12). On the contrary the normal force F_3 in the gap x0-x38 decreases with bigger gap values.

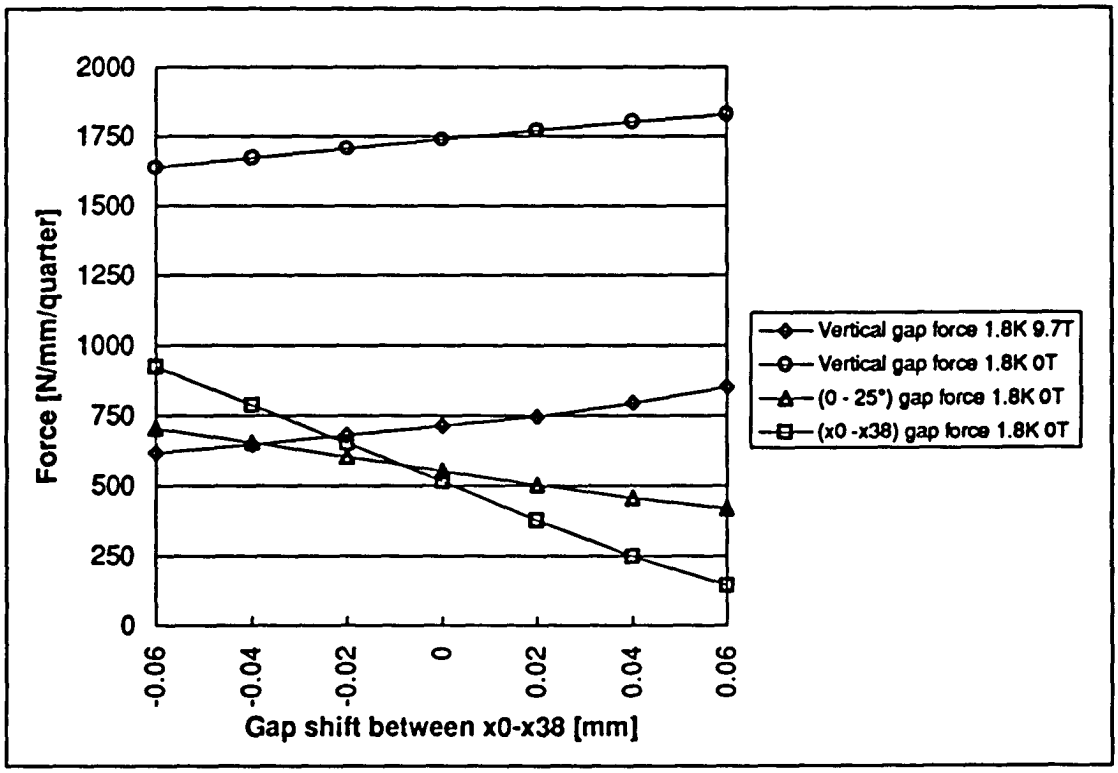

Figure 12. Normal contact forces vs. parallel gap shift between x0-x38. Nominal gap size is 0.2mm.

The influence of the vertical gap between yoke halves is illustrated in fig. 13. Vertical gap has been moved parallel around the nominal dimensions. Forces behave linearly at 1.8K. At the 9.7T vertical gap starts to lose

contact in some points when the gap size is increased. This can be seen as a nonlinear behavior that starts when the gap value is 0.03mm bigger than the nominal value. Correspondingly the normal force F_1 behaves non-linearly at 1.8K

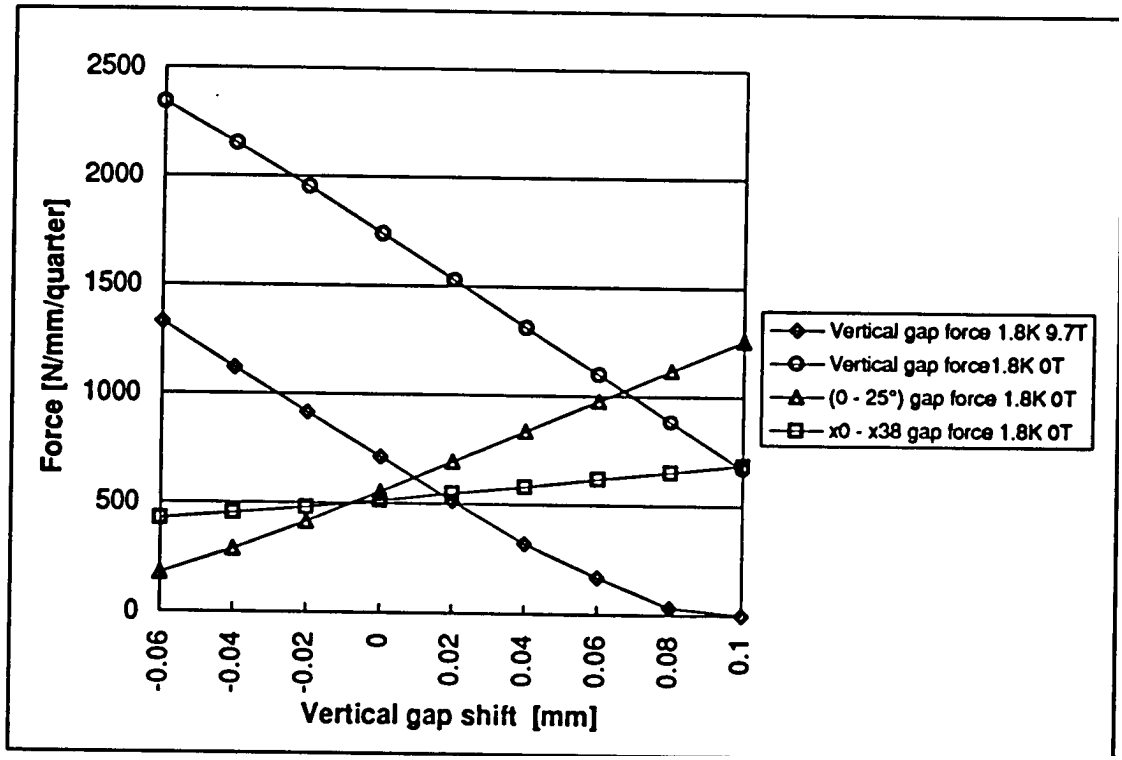

Figure 13. Normal contact forces vs. Parallel vertical gap shift
Between Di-Do. Nominal gap size is at D_i 0.47 mm at D_0 0.62 mm.

Figure 14 presents the influence of the prestress on the normal forces F_1 and F_3 between collar yoke interface and on the yoke gap mating force F_g. At the room temperature a change of the prestress in the shrinking cylinder is taken wholly by the collars because of the open vertical yoke gap. At the low temperature mating force F_g changes linearly with pestress and has very little effect on the forces F_1 and F_3 since the vertical gap remains closed. When the magnet is energized F_g decreases while correspondingly F_1 and F_3 increase under the influence of the Lorentz forces.

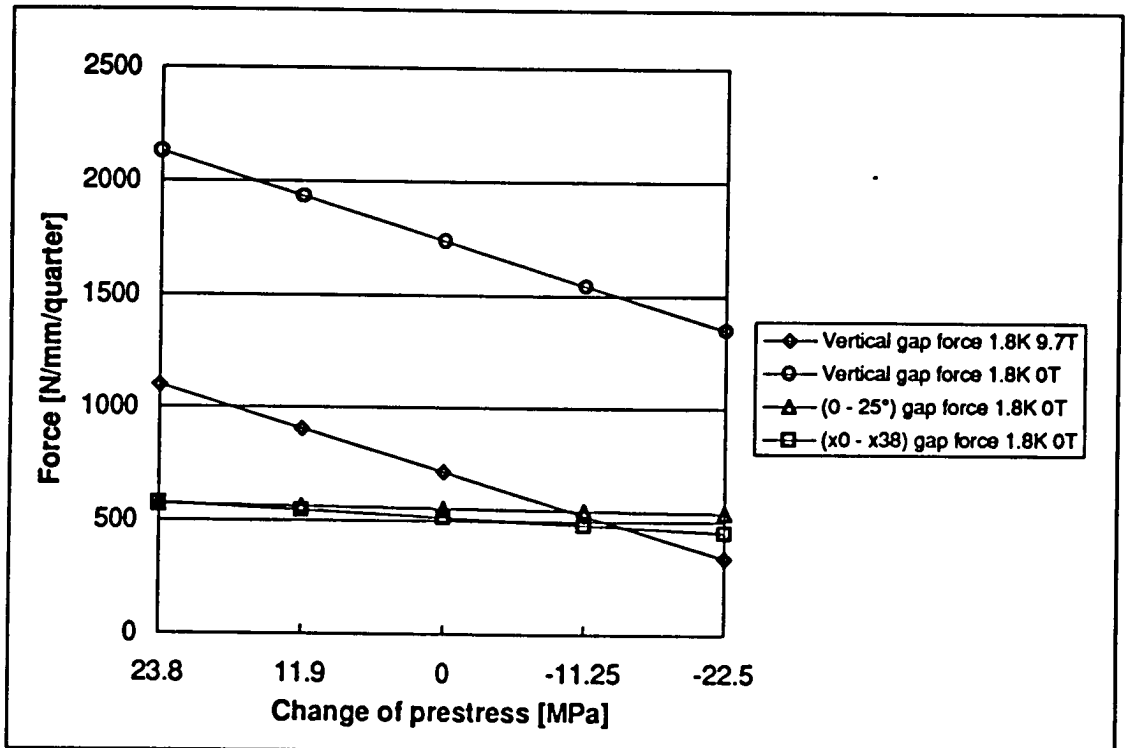

Figure 14. Normal contact forces between surfaces vs. the change of the shrinking cylinder prestress. Nominal prestress is 156MPa at 293K.

For small gap shifts around the nominal dimensions, one can get, for a certain force F_i:

$$F_i = F_{i0} + \sum \frac{\partial F_i}{\partial Gap_j} \cdot dGap_j \,,$$

where every differential term can be evaluated as the "slope" of the curve representing the force i vs. the gap j shift. If the variations are small around nominal dimensions, forces behave linearly as the function of the tolerances. We can therefore define a matrix of the slopes [S]:

$$[F] = [S] \cdot [u] + [F_0],$$

where [u] are the shifts [mm], [F] the forces [N/mm] due to these shifts and $[F_0]$ the forces [N/mm] due to the nominal gaps values. The influence of vertical gap, (0^0-25^0) gap and (x0-x38) gap shifts on the corresponding mating forces can be evaluated using the following matrix:

$$[S] = \begin{bmatrix} -10150 & 1675 & 6450 \\ 1525 & -6825 & -2525 \\ 6625 & -2500 & -7875 \end{bmatrix} \quad [\mathrm{N/mm^2}]$$

and the complete equation:

$$\begin{bmatrix} F_{VertGap} \\ F_{(x0-x38)Gap} \\ F_{(0°-25°)Gap} \end{bmatrix} = \begin{bmatrix} -10150 & 1675 & 6450 \\ 1525 & -6825 & -2525 \\ 6625 & -2500 & -7875 \end{bmatrix} \cdot \begin{bmatrix} \Delta_{VertGap} \\ \Delta_{(x0-x38)Gap} \\ \Delta_{(0°-25°)Gap} \end{bmatrix} + \begin{bmatrix} 713 \\ 513 \\ 552 \end{bmatrix} \quad [\mathrm{N/mm}].$$

In table 7 we defined two 'bad cases'. In the first case the normal contact force F_1 between collars and yoke has been minimized by choosing all the tolerances in a unfavorable way. In the second case the vertical mating force F_z has been minimized. Results have been compared with ANSYS to check the accuracy of the estimation. We can see reasonable correspondence, except normal force F_1 with very low values, when simplified model is over pessimistic. This can be explained by the fact that the forces in this region behave unlinearly with low force levels, as it can be seen from the figures 11 and 13. Due to the approximations of the model a reasonable safety margin has to be considered. This is the reason why far from the nominal conditions low forces are less interesting.

	Shift [mm]	ΔF_z [N/mm] (1.8K, 9.7T)	ΔF_1 [N/mm] (1.8K)	ΔF_3 [N/mm] (1.8K)
Vertical gap	-0.04	+406	-265	-61
0°-25° gap	0.02	+129	-157.5	-50.5
x0-x38	0.03	+50.2	-75	-204.7
Nominal force		713	552	513
Estimated force		1298.2	54.5	196.7
ANSYS		1294	112.5	219.9
Error		0.3 %	-51.5%	-10.5%
Vertical gap (F_z)	0.04	-406	+265	+61
0°-25° gap (F_1)	-0.02	-129	+157.5	+50.5
x0-x38 (F_3)	-0.03	-50.2	+75	+204.7
Nominal force		713	552	513
Estimated force		127.8	1049.5	829.2
ANSYS		145	1069	839
Error		-11.9 %	-1.8 %	-1.2 %

Table 7. Acceptable 'worst cases'. Influences of the different tolerances have been summed up. Results have been compared with ANSYS.

8.ERRORS

ANSYS program calculates a structural energy error for each element which is the measure of discontinuity of the stress field from element to element. This discrepancy is due to the assumption in the elements that only the displacements are continuous at the nodes. The stress field is calculated from the displacements and should also be continuous, but generally is not.

Optimum result can be obtained when energy error norm is constant over the whole model. In the model, high energy error norms occur near highly stressed places e.g. near key pin holes and in some shrinking cylinder elements. This means that the meshing should be more dense in these particular areas. Unfortunately it is not possible to create much denser mesh, because the size of the database is already very close to the allowable limits of the used ANSYS-version, particularly in the load case with the Lorentz forces. Energy error norm for the model is presented in appendix (fig. 24-27).
The dark areas represents the places in which the computed stresses are affected by the biggest errors.

ACKNOWLEDGEMENT

The authors wish to thank R. Perin for his valuable advises and suggestions.

REFERENCES

1. Bona M., Perini D., Finite element structural analysis of the twin aperture prototype superconducting magnet for the large hadron collider. Geneva 1990, CERN, LHC Note 120

2. ANSYS User's Manual for Revision 5.0, Houston 1992, Swanson Analysis Systems Inc.

3. Design features of the new LHC dipole long models (prototypes). Edited by Perin, R. Geneva 1994, CERN, Internal Note 94-103

4. Meβ K. H., Schmuser P., Superconducting Accelerator magnets, Superconductivity in particle accelerators, CAS CERN Accelerator school, Geneva 1989.

APPENDIX

Stresses and displacements plots.

Azimuthal stresses in the fixed collar when the collaring force is applied

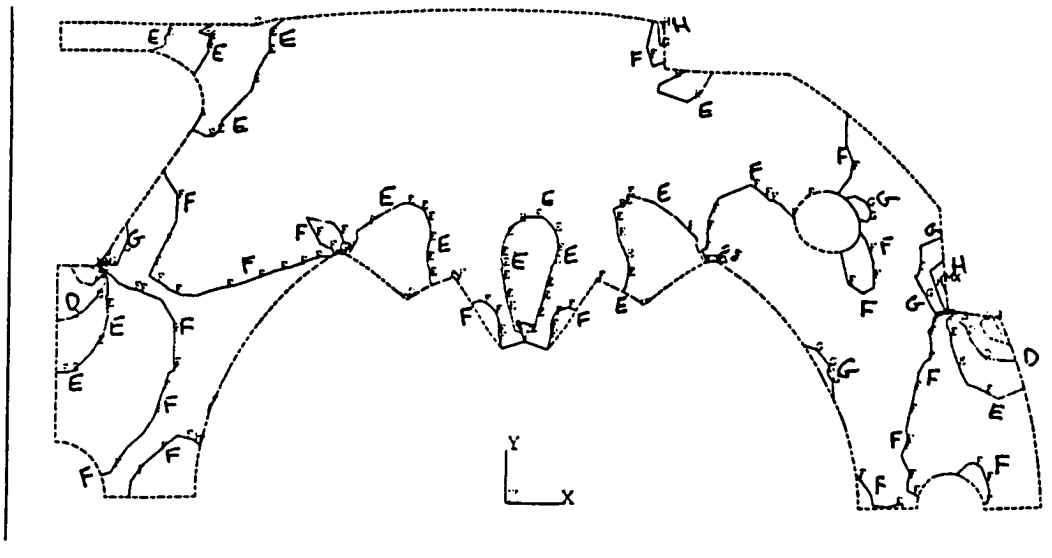

Fig. 1

Radial stresses in the fixed collar when the collaring force is applied

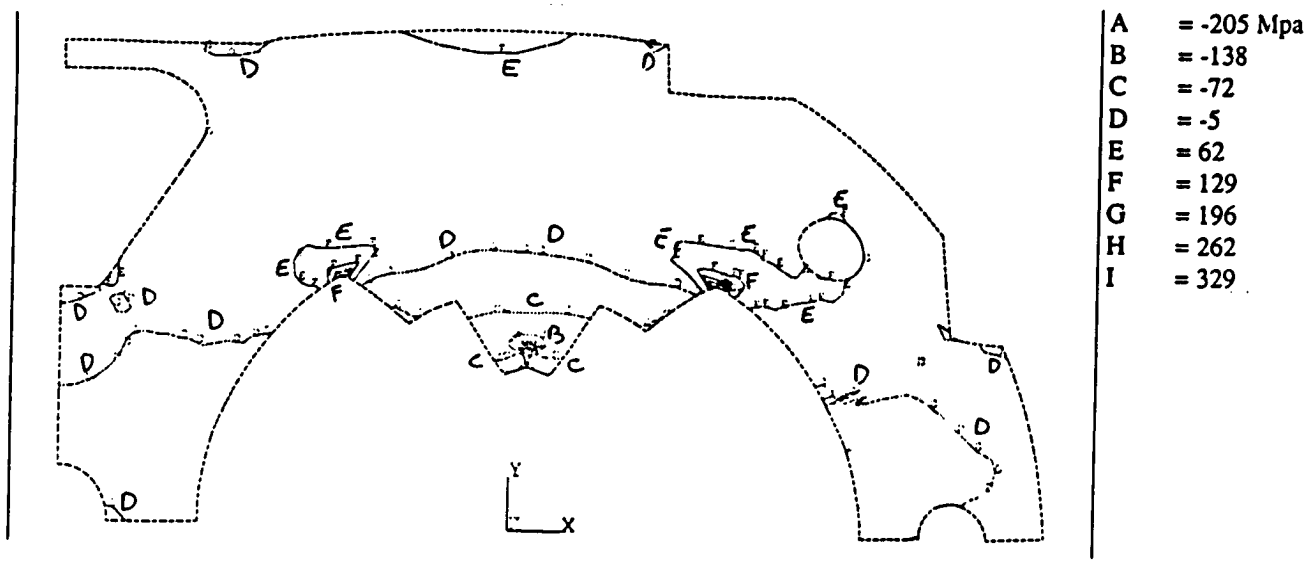

Azimuthal stresses in the coil after the collaring

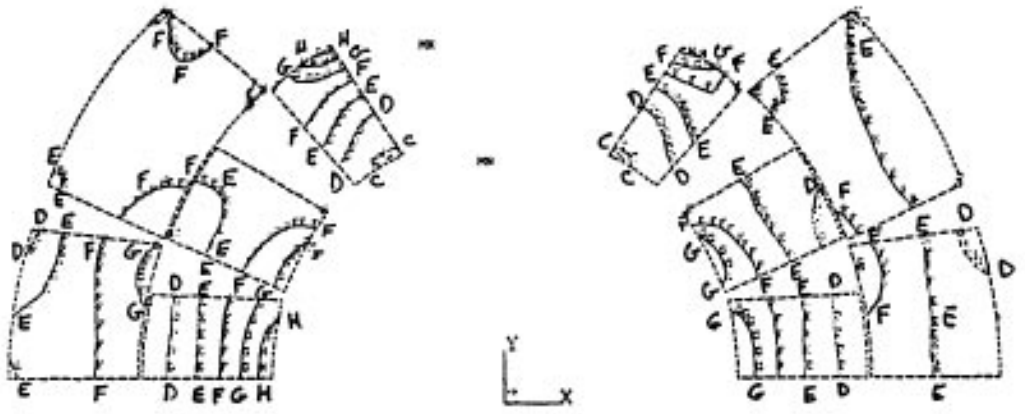

Fig. 3

Azimuthal stresses in the fixed collar after the collaring

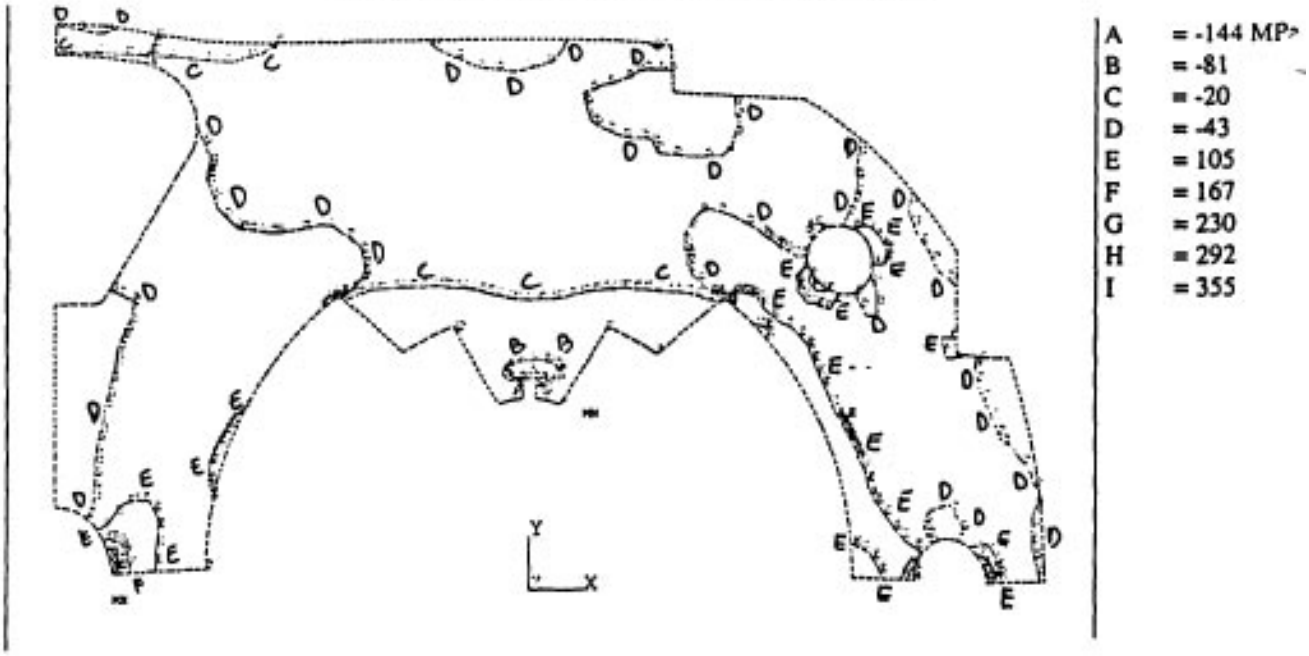

Fig. 4

Radial stresses in the fixed collar after the collaring

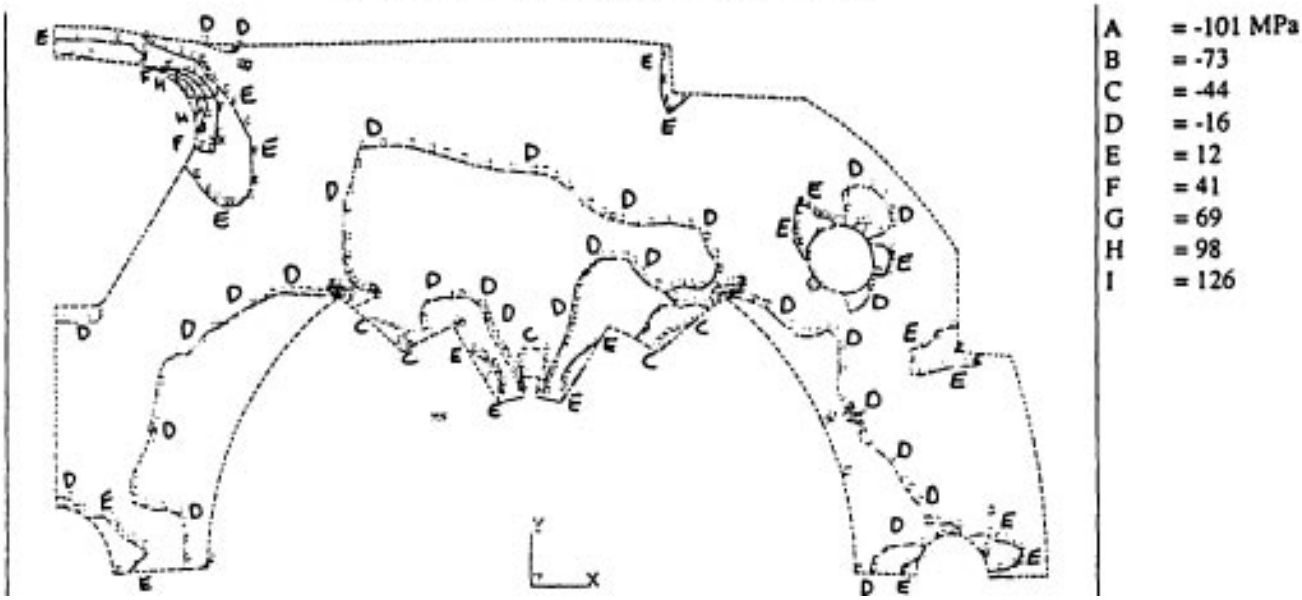

Horizontal displacements in the fixed collar after the collaring

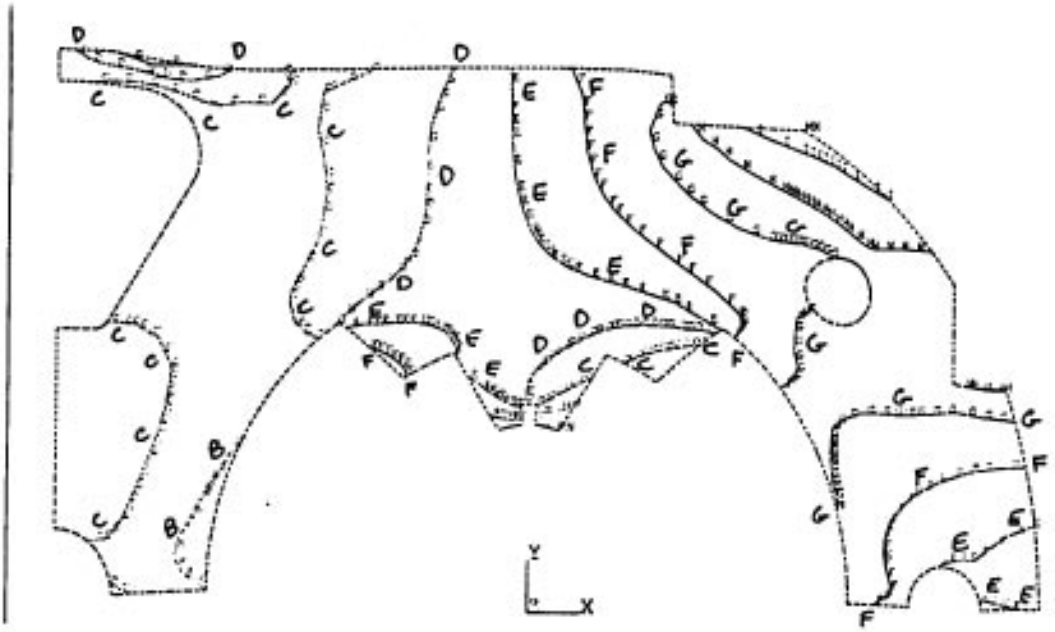

Fig. 6

Vertical displacements in the fixed collar after the collaring

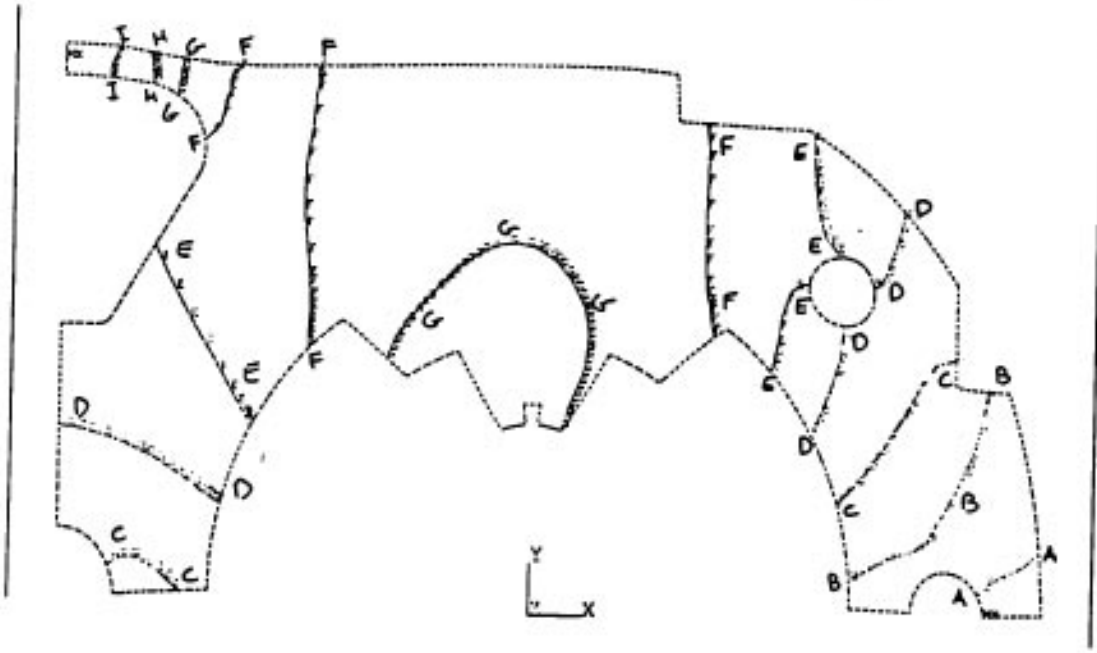

Fig. 7

Azimuthal stresses in the coil at 293K

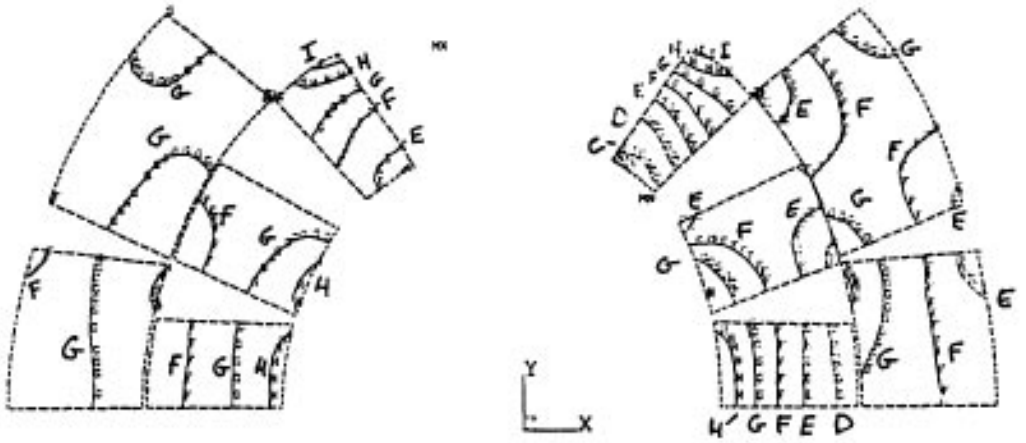

Fig. 8

Azimuthal stresses in the fixed collar at 293K

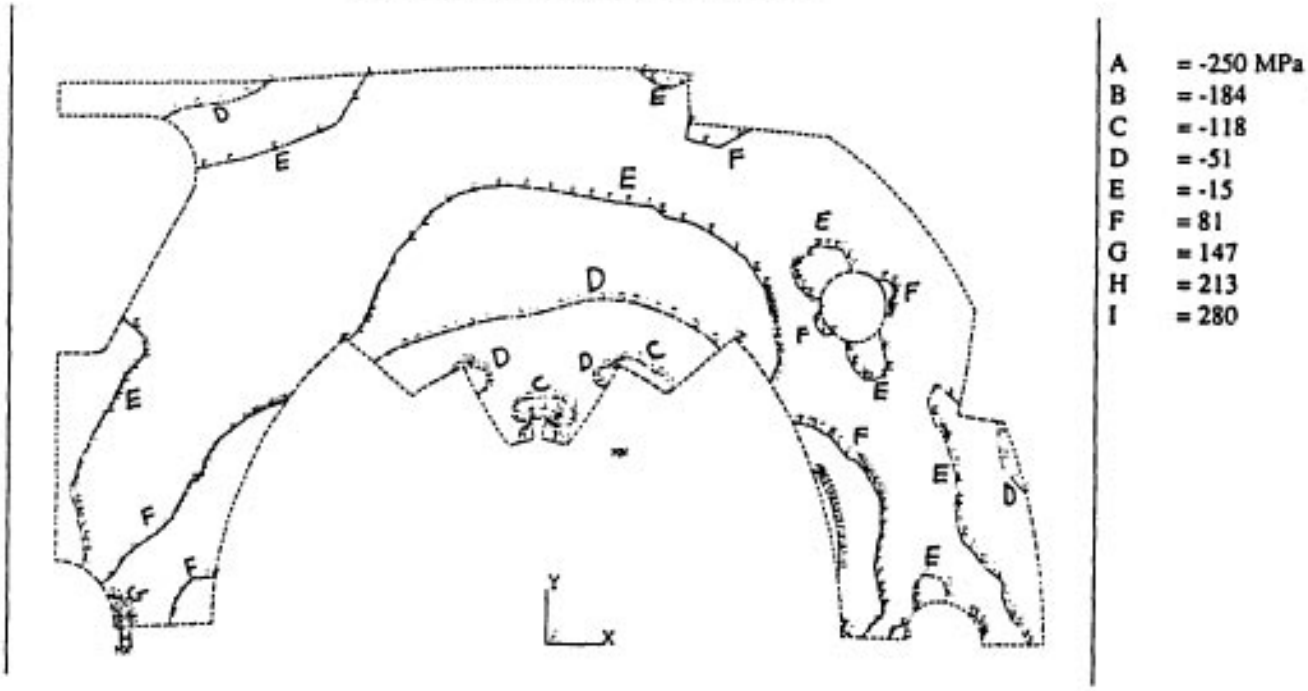

Fig. 9

Radial stresses in the fixed collar at 293K

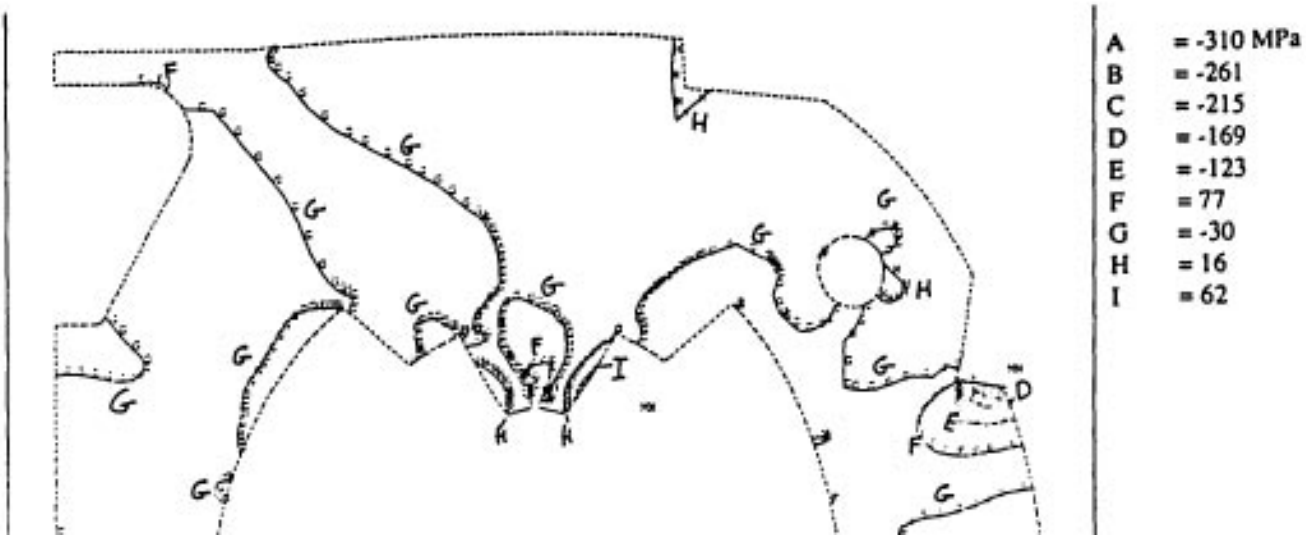

Von Mises stresses in the yoke at 293K

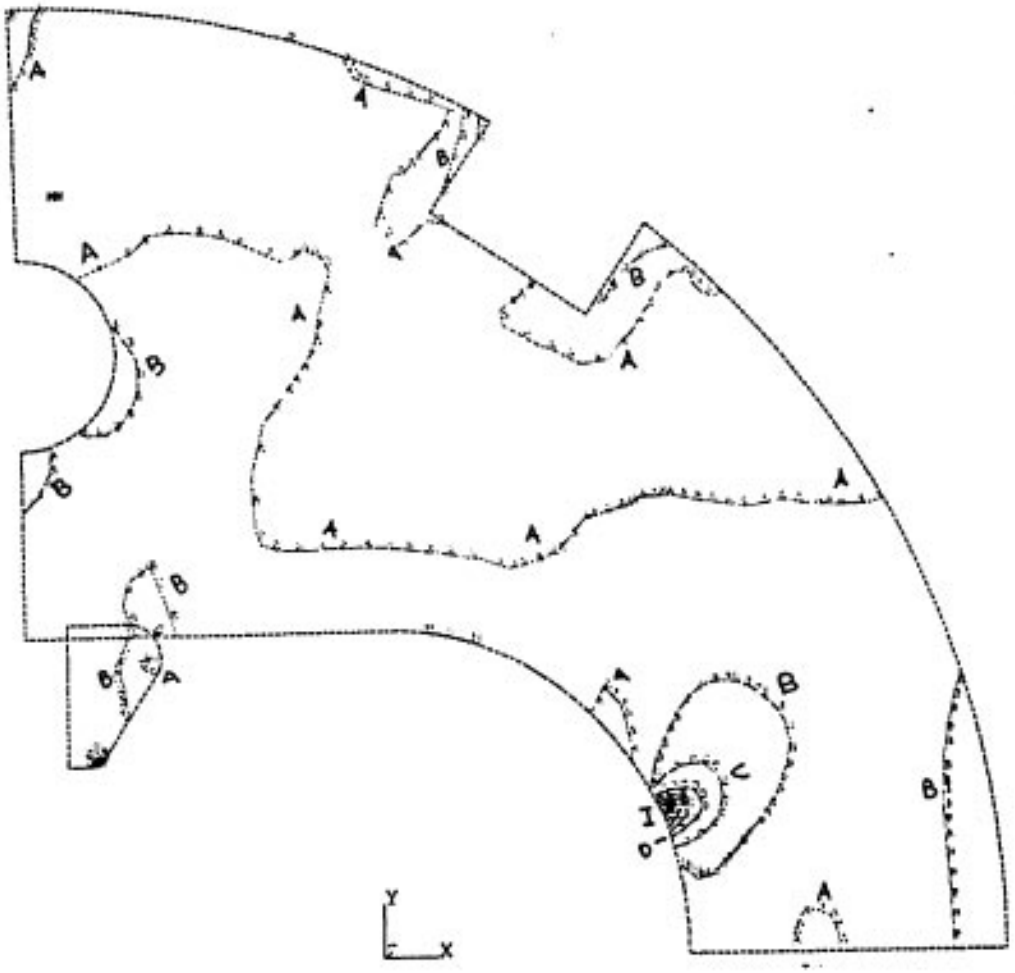

A	= 11 MPa
B	= 32
C	= 52
D	= 73
E	= 94
F	= 114
G	= 136
H	= 156
I	= 177

Fig. 11

Azimuthal stresses in the shrinking cylinder at 293 K

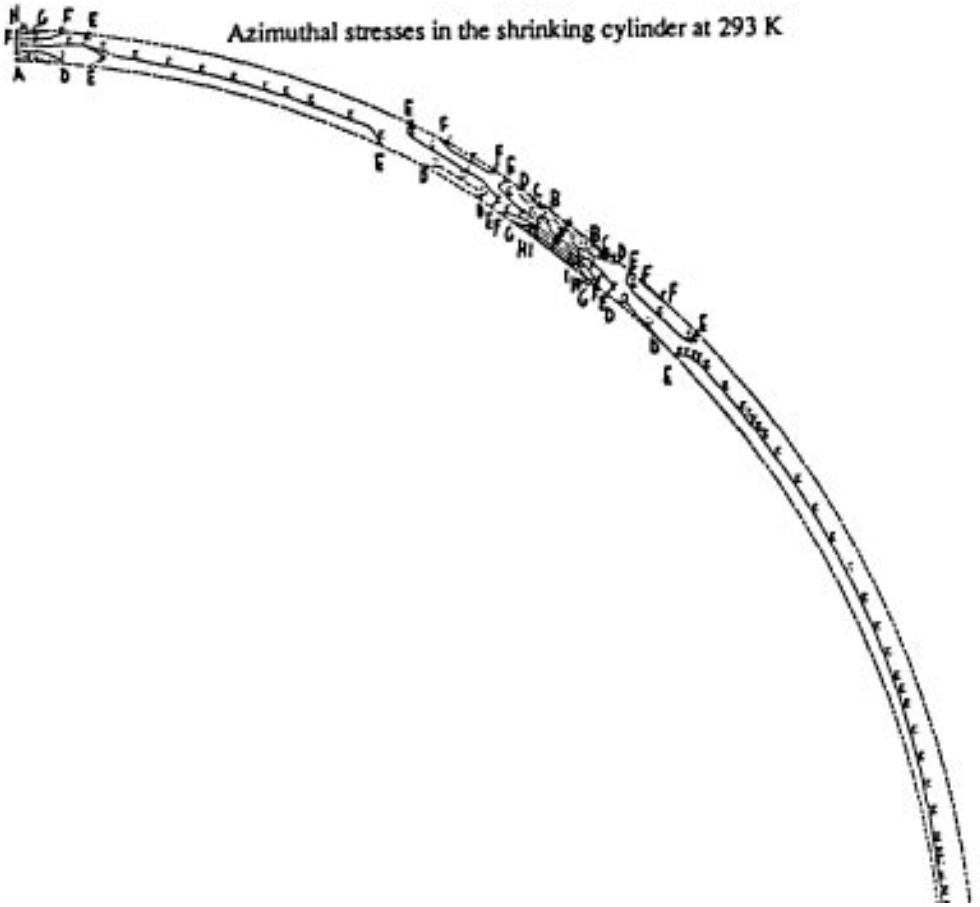

A	= 102 Mpa
B	= 115
C	= 129
D	= 142
E	= 155
F	= 169
G	= 182
H	= 195
I	= 209

Azimuthal stresses in the coil at 1.8K

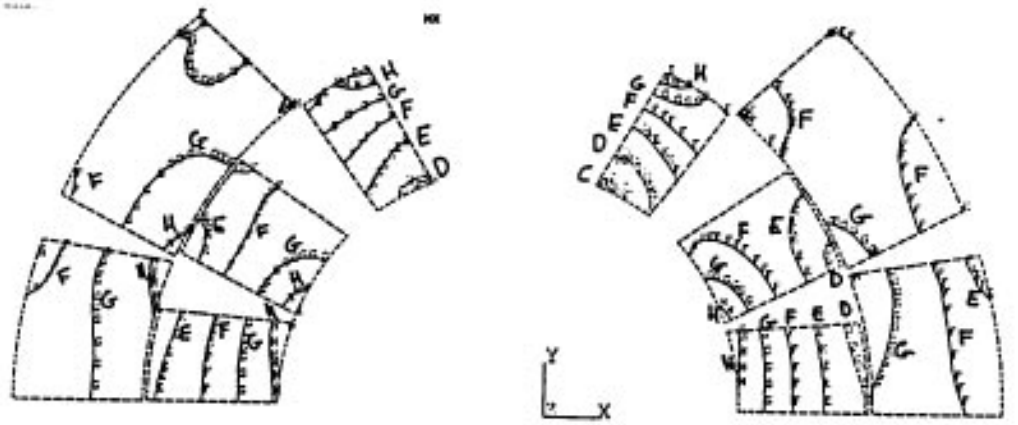

Fig. 13

Azimuthal stresses in the fixed collar at 1.8K

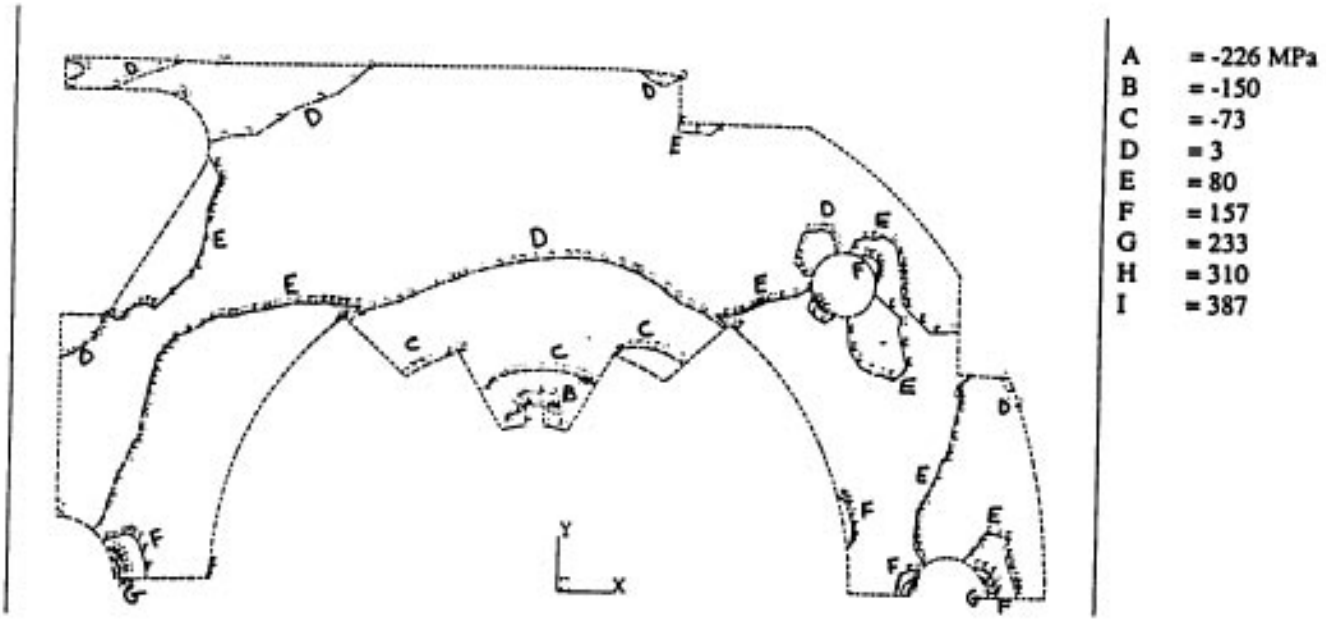

Fig. 14

Radial stresses in the fixed collar at 1.8K

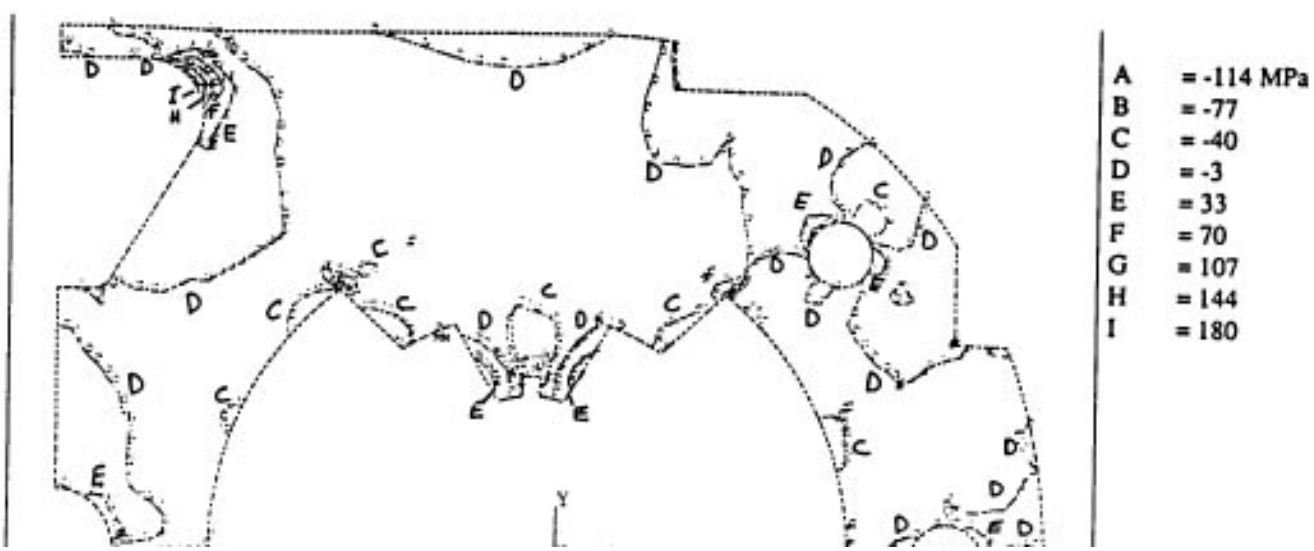

Von Mises stresses in the yoke at 1.8K

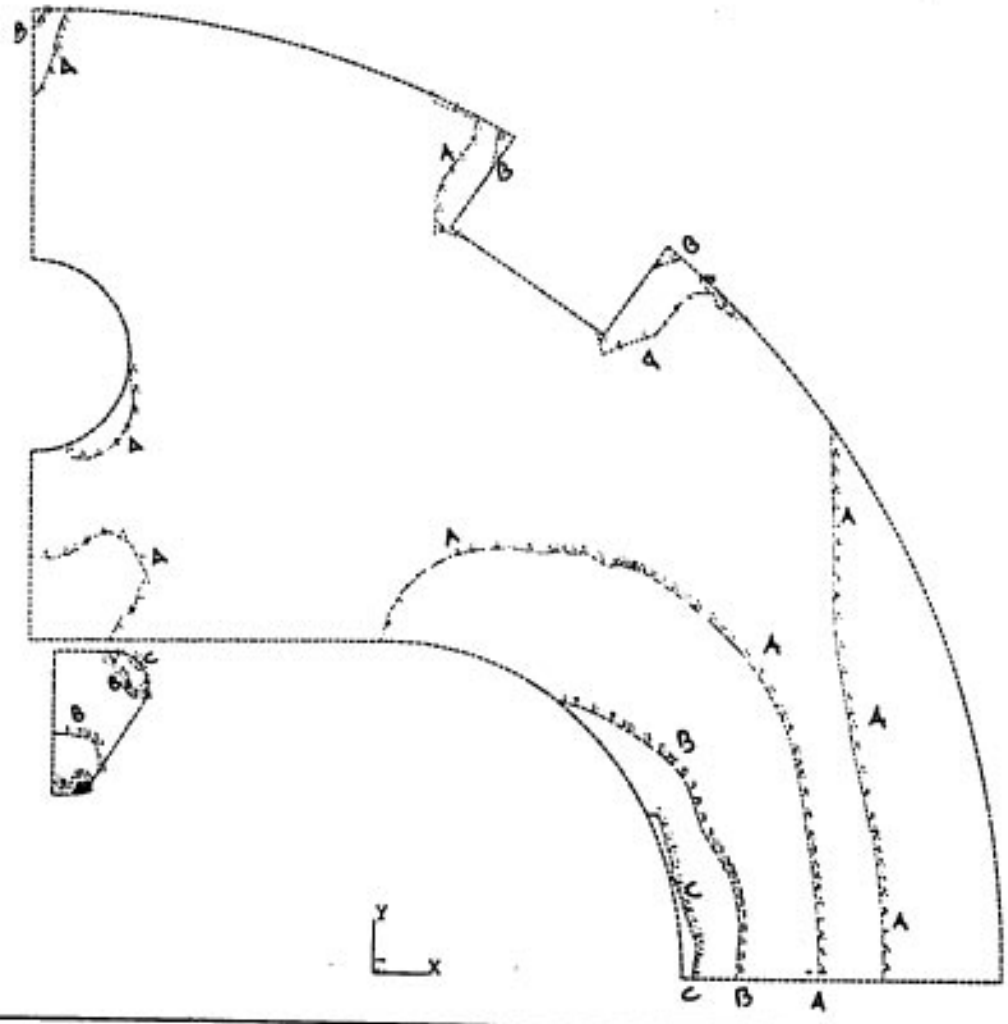

A	= 20 MP
B	= 59
C	= 100
D	= 137
E	= 176
F	= 215
G	= 253
H	= 292
I	= 331

Fig. 16

Azimuthal stresses in the shrinking cylinder at 1.8 K

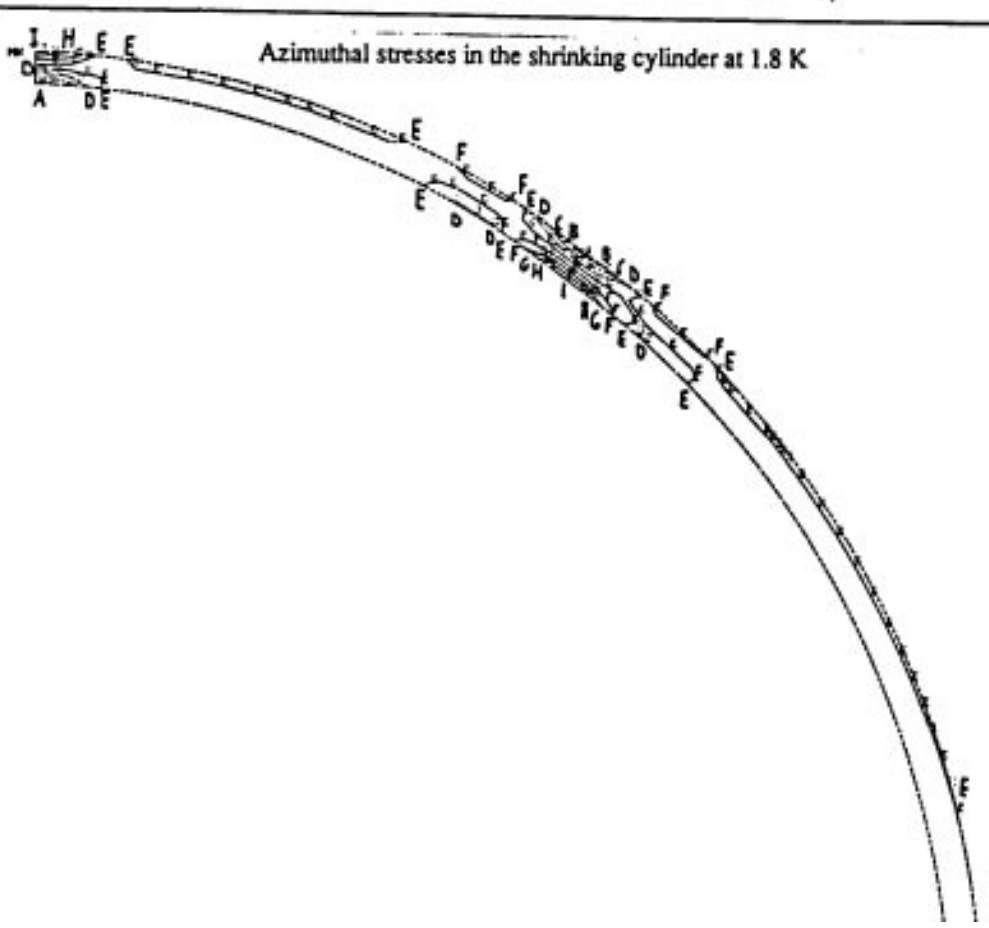

A	= 128 Mp
B	= 152
C	= 175
D	= 198
E	= 221
F	= 245
G	= 268
H	= 291
I	= 314

Azimuthal stresses in the coil at 9.7T

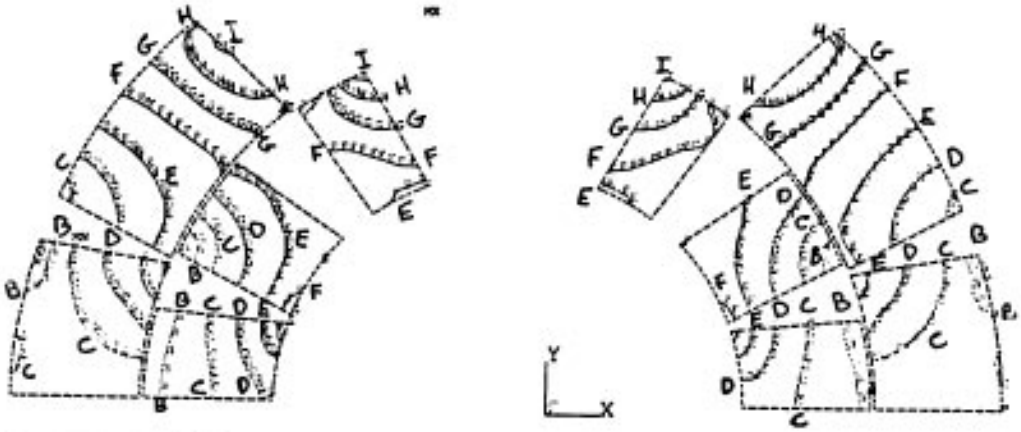

Fig. 18

Azimuthal stresses in the fixed collar at 9.7T

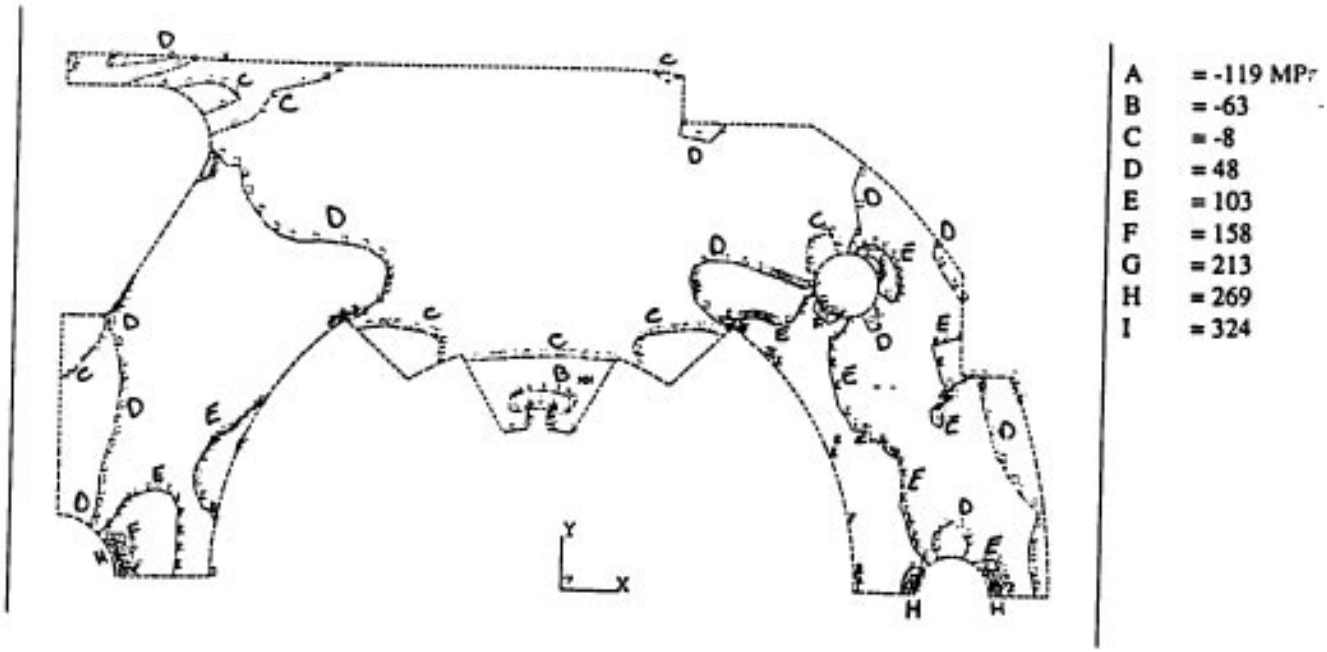

g. 19

Radial stresses in the fixed collar at 9.7T

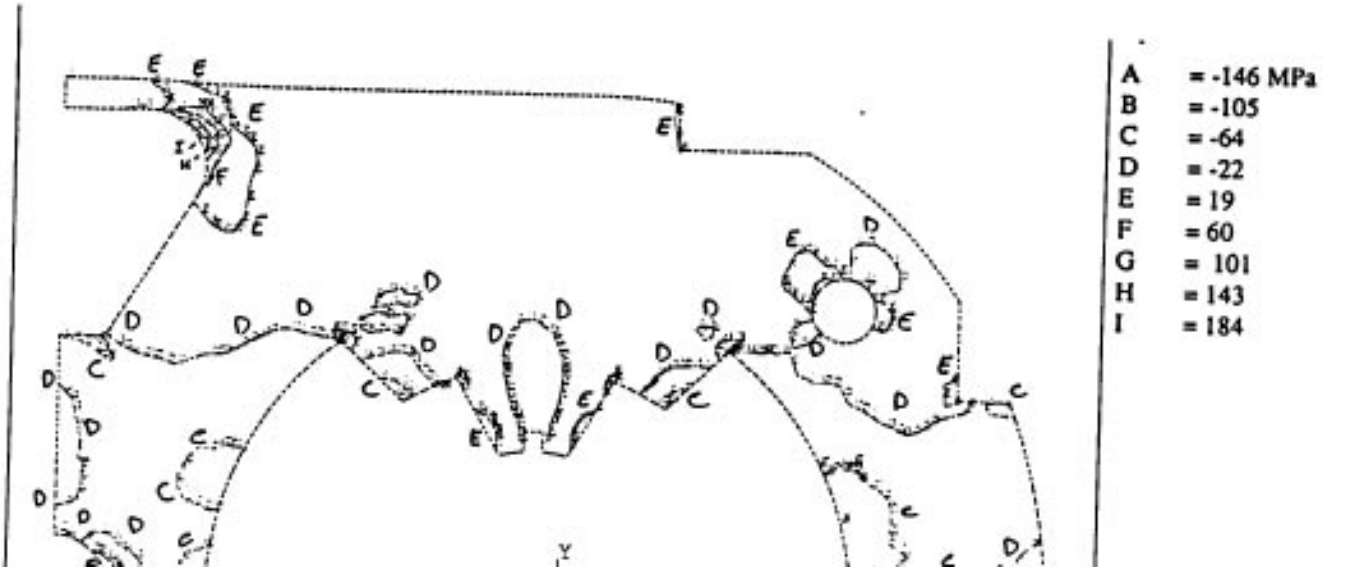

Von Mises stresses in the yoke at 9.7T

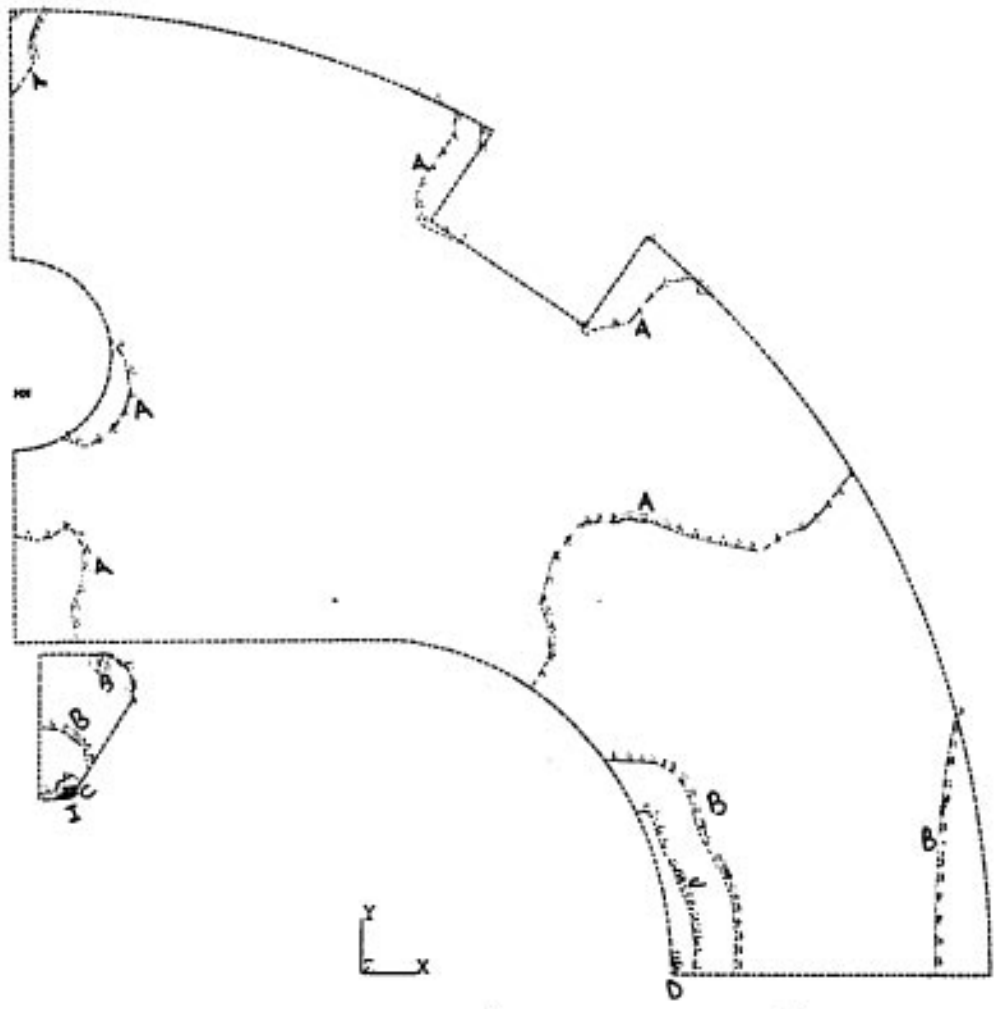

A	= 24 MPa
B	= 68
C	= 112
D	= 156
E	= 200
F	= 244
G	= 289
H	= 333
I	= 377

Fig. 21

Azimuthal stresses in the shrinking cylinder at 9.7 K

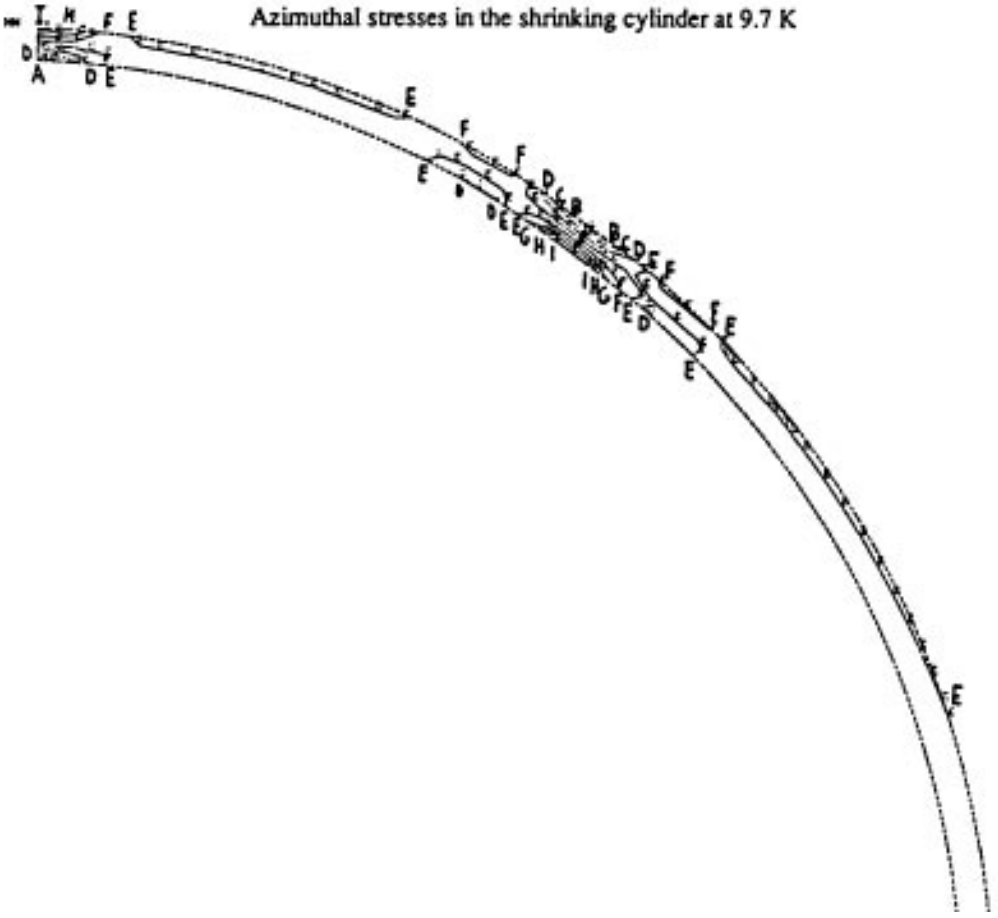

A	= 131 Mp
B	= 154
C	= 176
D	= 199
E	= 222
F	= 244
G	= 267
H	= 289
I	= 312

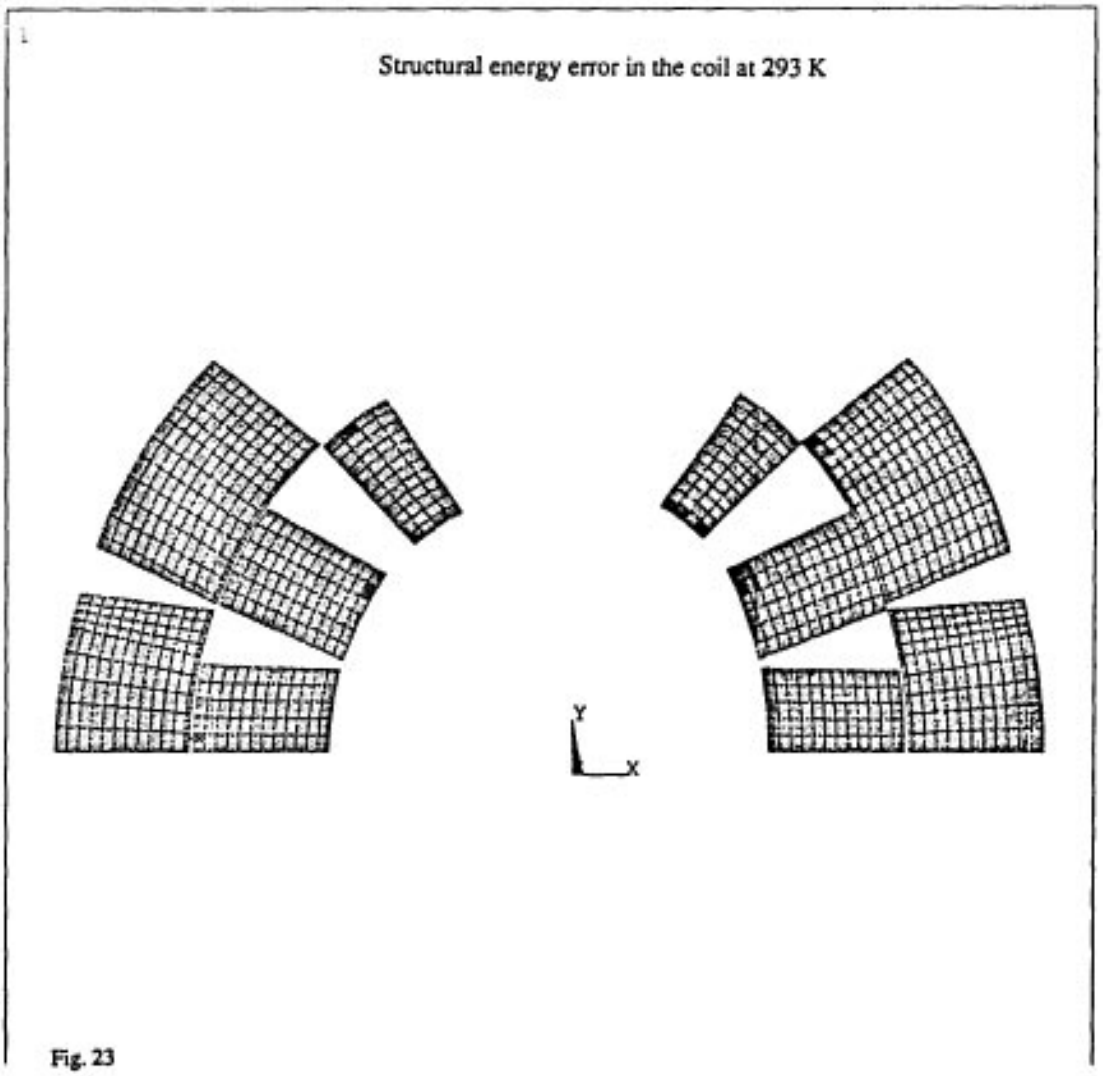
Structural energy error in the coil at 293 K
ANSYS 5.0 A
FEB 27 1995
13:17:17
PLOT NO. 1
ELEMENT SOLUTION
STEP=1
SUB =10
TIME=1
SERR
DMX =.249778
SMN =.601E-05
SMX =.032935
.601E-05
.003665
.007324
.010982
.014641
.0183
.021959
.025618
.029276
.032935
Y
X

Fig. 23

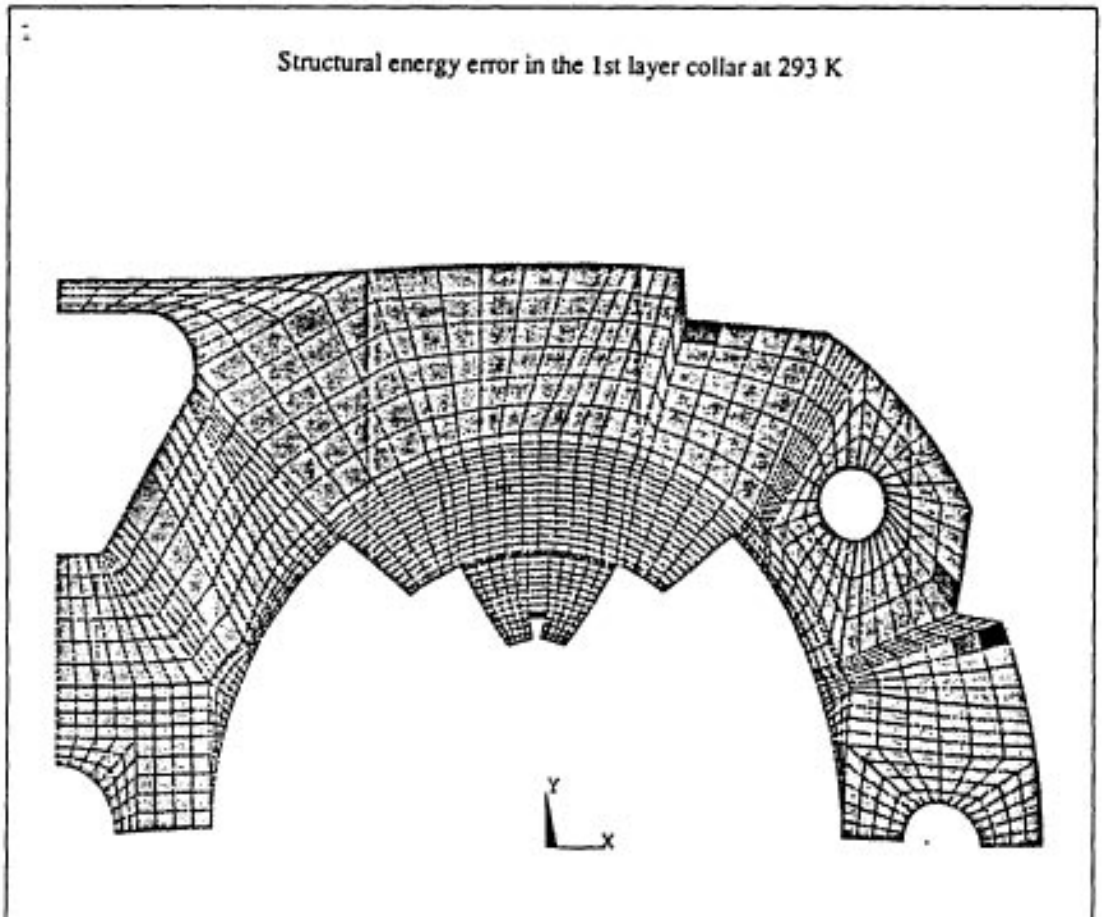
Structural energy error in the 1st layer collar at 293 K
ANSYS 5.0 A
FEB 27 1995
13:17:28
PLOT NO. 3
ELEMENT SOLUTION
STEP=1
SUB =10
TIME=1
SERR
DMX =.261858
SMN =.130E-05
SMX =.407848
.130E-05
.045318
.090634
.13595
.181267
.226583
.271899
.317215
.362532
.407848
Y
X

Structural energy error in the yoke at 293 K

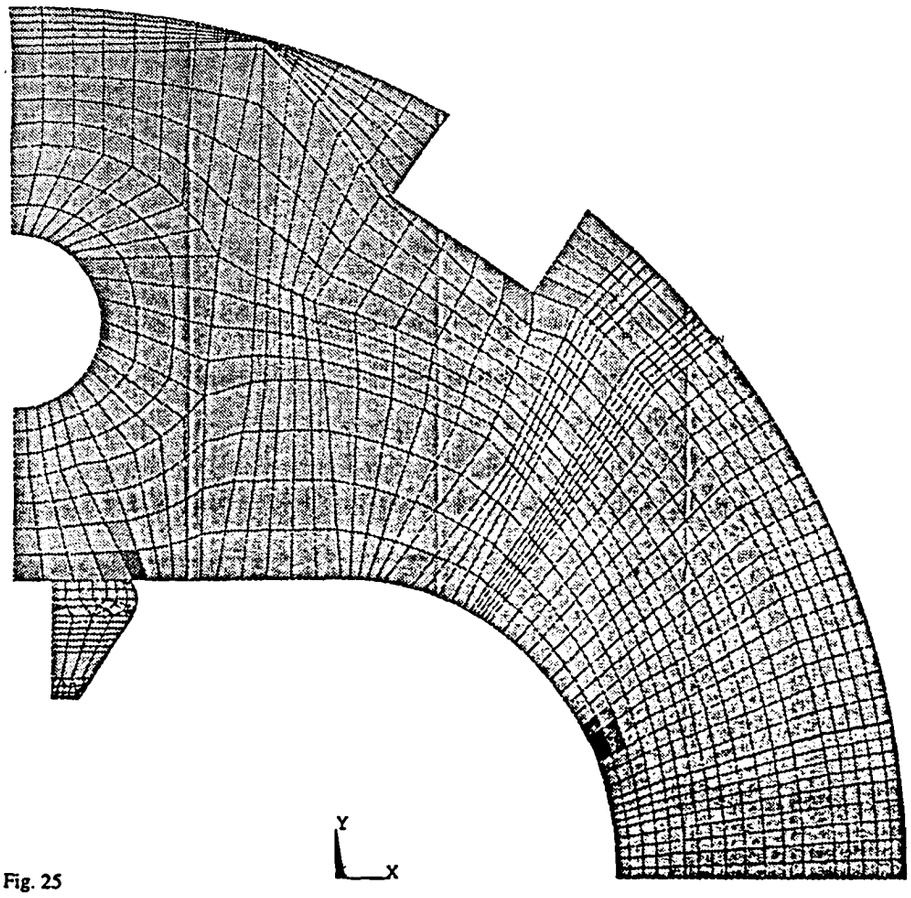

ANSYS 5.0 A
FEB 27 1995
13:17:34
PLOT NO. 4
ELEMENT SOLUTION
STEP=1
SUB =10
TIME=1
SERR
DMX =.27563
SMN =.777E-06
SMX =.195101
.777E-06
.021679
.043356
.065034
.086712
.10839
.130068
.151746
.173424
.195101

Fig. 25

Structural energy error in the shrinking cylinder at 293 K

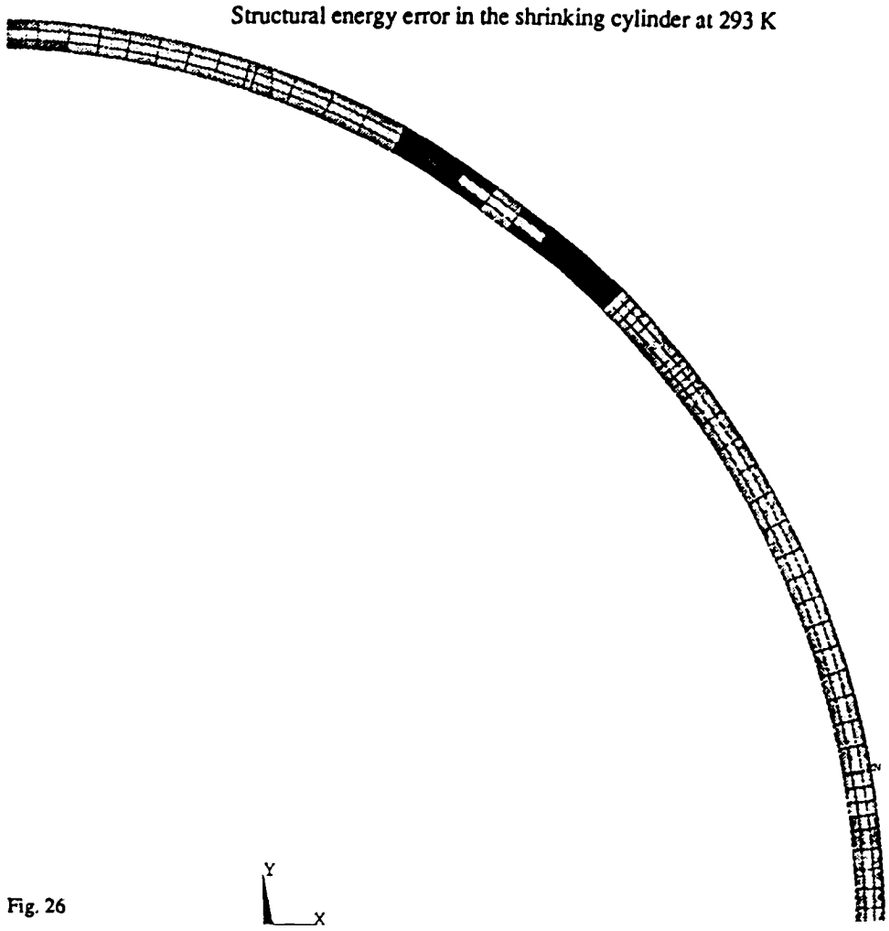

ANSYS 5.0 A
FEB 27 1995
17:59:02
PLOT NO. 1
ELEMENT SOLUTION
STEP=1
SUB =10
TIME=1
SERR
DMX =.344951
SMN =.137E-04
SMX =.047851
.137E-04
.005329
.010644
.01596
.021275
.02659
.031905
.037221
.042536
.047851

Fig. 26